SKB

TECHNICAL REPORT 94-30

Calibration with respect to hydraulic head measurements in stochastic simulation of groundwater flow – A numerical experiment using MATLAB

L.O. Eriksson, J Oppelstrup

Starprog AB

December 1994

SVENSK KÄRNBRÄNSLEHANTERING AB
SWEDISH NUCLEAR FUEL AND WASTE MANAGEMENT CO

BOX 5864 S-102 40 STOCKHOLM
TEL. 08-665 28 00 TELEX 13108 SKB
TELEFAX 08-661 57 19

CALIBRATION WITH RESPECT TO HYDRAULIC HEAD MEASUREMENTS IN STOCHASTIC SIMULATION OF GROUNDWATER FLOW - A NUMERICAL EXPERIMENT USING MATLAB

L.O. Eriksson, J Oppelstrup

Starprog AB

December 1994

This report concerns a study which was conducted for SKB. The conclusions and viewpoints presented in the report are those of the author(s) and do not necessarily coincide with those of the client.

Information on SKB technical reports from1977-1978 (TR 121), 1979 (TR 79-28), 1980 (TR 80-26), 1981 (TR 81-17), 1982 (TR 82-28), 1983 (TR 83-77), 1984 (TR 85-01), 1985 (TR 85-20), 1986 (TR 86-31), 1987 (TR 87-33), 1988 (TR 88-32), 1989 (TR 89-40), 1990 (TR 90-46), 1991 (TR 91-64), 1992 (TR 92-46) and 1993 (TR 93-34) is available through SKB.

Calibration with respect to hydraulic head measurements in stochastic simulation of groundwater flow - a numerical experiment using MATLAB

L.O. Eriksson, J. Oppelstrup
Starprog AB

December 1994

Keywords: groundwater flow, hydraulic head, hydraulic conductivity, stochastic simulation, calibration, inverse modelling, kriging.

Abstract (English)

A simulator for 2D stochastic continuum simulation and inverse modelling of groundwater flow has been developed. The simulator is well suited for method evaluation and what-if simulation and written in MATLAB. Conductivity fields are generated by unconditional simulation, conditional simulation on measured conductivities and calibration on both steady-state head measurements and transient head histories. The fields can also include fracture zones and zones with different mean conductivities. Statistics of conductivity fields and particle travel times are recorded in Monte-Carlo simulations.
The calibration uses the pilot point technique, an inverse technique proposed by RamaRao and LaVenue. Several Kriging procedures are implemented, among others Kriging neighbourhoods. In cases where the expectation of the log-conductivity in the truth field is known the non-bias condition can be omitted, which will make the variance in the conditionally simulated conductivity fields smaller.

A simulation experiment, resembling the initial stages of a site investigation and devised in collaboration with SKB, is performed and interpreted.
The results obtained in the present study show less uncertainty than in our preceding study. This is mainly due to the modification of the Kriging procedure but also to the use of more data. Still the large uncertainty in cases of sparse data is apparent. The variogram represents essential characteristics of the conductivity field. Thus, even unconditional simulations take account of important information. Significant improvements in variance by further conditioning will be obtained only as the number of data becomes much larger.

Abstract (Swedish)

En simulator för stokastisk kontinuum-simulering och inversmodellering av 2D grundvattenströmning har utvecklats. Den är väl lämpad för metodutvärdering och "what-if" simulering och skriven i MATLAB. Konduktivitetsfält genereras med obetingad simulering, betingad simulering på uppmätta konduktiviteter och kalibrering på uppmätta stationära och transienta potentialer. Fälten kan innehålla sprickzoner och zoner med andra medelkonduktiviteter. Statistik på konduktivitetsfält och transporttider för partiklar registreras i Monte-Carlo-simuleringar.
Kalibreringen görs med pilot-punktsmetoden, en inversteknik föreslagen av RamaRao och LaVenue. Flera "Kriging"-förfaranden har implementerats, bl. a. "Kriging neighbourhoods". I fall där väntevärdet för log-konduktiviteten i sanningsfältet är känd, behöver väntevärdesriktigheten inte explicit krävas, vilket medför att variansen i de betingade konduktivitetsfälten blir mindre.

Ett simuleringsexperiment, beskrivande initialskedet vid en platsundersökning och utformat i samarbete med SKB, har genomförts och tolkats. De erhållna resultaten visar mindre osäkerhet än i vår tidigare studie. Detta beror huvudsakligen på modifieringen av "Kriging"-förfarandet och på att mer data har använts. Fortfarande är dock den stora osäkerheten i fall med glesa data tydlig. Variogrammet fångar många av de viktigaste egenskaperna hos konduktivitetsfältet. Det betyder att även obetingad simulering i själva verket tar hänsyn till viktig information. Signifikant minskning i variansen genom ytterligare betingning fås bara om mängden data ökas betydligt.

Table of Contents

page
Summary ii
1. Introduction 1
2. Mathematical Model 4
2.1 Groundwater Flow Equation 4
2.2 Variogram 5
3. Solution technique 6
3.1 Discretization 6
3.2 Simulation of conductivities 7
3.2.1 Unconditional simulation 7
3.2.2 Conditional simulation 8
3.3 Calibration 10
3.3.1 Objective function 11
3.3.2 Minimization 12
3.3.3 Gradient computation 12
3.4 Particle tracking 16
4. Computer implementation 18
4.1 Flowchart 18
4.2 MATLAB 19
4.3 Verification experiment 19
4.3.1 Deterministic verification of steady-state calibration 19
4.4 Comparison with pilot point technique by RamaRao & LaVenue 21
5. Simulation experiment 24
6. Results and discussion 34
6.1 Simulation experiment 34
6.2 Development of simulation tool 36
6.3 Inverse modelling by the Pilot point method 36
7. References 38
Appendix A Kriging procedures implemented 40
Appendix B An example of conditioning on more data 43
Appendix C Example of problem specification file 46

Summary

Stochastic continuum models for simulation of groundwater flow in fractured rock, where the flow in fractures is modeled by Darcian flow through a set of blocks, each having a constant bulk conductivity and storativity are used for waste repository site evaluation.

In unconditional simulation, the rock mass property is characterized only by statistical information. When specific measurements of conductivity, or other available data, such as recorded histories of hydraulic head and flow in boreholes are incorporated into the realizations of the fields in the Monte-Carlo simulations, we speak of conditional simulation.

In a former project, a simulation tool was built, suitable for "what-if" studies of how best to use such information in conditional simulations. The simulator is based on the "pilot point method" with inverse modeling and implemented in MATLAB. A simulation experiment devised in collaboration with SKB was then performed and interpreted.

The results obtained in that simulation experiment contributed to the understanding of how the information contained in the history data can be used, and of the limitations inherent in the large uncertainty in cases of sparse data, as the case will be for initial site evaluations planned by SKB. Some suggestions of how the kriging methodology used in the conditioning could be improved to decrease the uncertainty were also gained.

The aim of the present study is to further develop the simulation tool and to perform a simulation experiment with more but still realistically sparse data.

The 2D simulator for method evaluation and what-if simulation has been further developed in MATLAB. Conductivity fields are generated by unconditional simulation, conditional simulation on measured conductivities and calibration on both steady-state head measurements and transient head histories. The fields can also include fracture zones and zones with different mean conductivities. Statistics of conductivity fields and particle travel times are recorded in Monte-Carlo simulations.

Several kriging procedures are implemented, among others Kriging neighbourhoods. In cases where the expectation of the log-conductivity in the truth field is known the non-bias condition can be omitted, which

will make the variance in the conditionally simulated conductivity fields smaller.

The results obtained in the present study show less uncertainty than in our preceding study. This is mainly due to the modification of the Kriging procedure but also to the use of more data. Still the large uncertainty in cases of sparse data is apparent. The variogram represents essential characteristics of the conductivity field. Thus, even unconditional simulations take account of important information. Significant improvements in variance by further conditioning will be obtained only as the number of data becomes much larger.

1. Introduction

Simulation of groundwater flow in fractured rock is a key tool for waste repository site assessment. One of the approaches in use is the stochastic continuum model where the flow in fractures is modeled by Darcian flow through a set of blocks, each having a constant bulk conductivity and storativity. The property of greatest interest here is the bulk conductivity of the blocks.

Monte-Carlo simulations are carried out to find the distribution and envelope of flow fields compatible with both statistical information and more specific site data. In unconditional simulation, the rock mass property is characterized only by statistical information, such as mean, pointwise distribution, and moments of two-point correlation functions, the spatial variogram. One usually assumes that conductivity has a log-normal distribution.

When specific measurements of conductivity, or other available data such as recorded histories of hydraulic head and flow in boreholes, are incorporated into the realizations of the fields in the Monte-Carlo simulations we speak of conditional simulations.

How best to use the information available in conditional simulations is the subject of much research. de Marsily, Neumann & Carrera, and LaVenue and RamaRao, (ref.[1], [2], [3], [15]), have proposed many of the techniques now in use. It is the purpose of this investigation to develop tools to help in understanding and assessing such proposals, the goal being an incorporation of the most efficient techniques into the SKB Waste Repository Assessment codes.

In particular, the use of recorded head histories in interference pumping tests by inverse modeling requires substantial computer resources and code development and adaptation.

It was decided that in-house competence and development management would be best served by building a simulation tool for "what-if" simulations which would be flexible and general enough to allow substantial experimentation. The simulation tool was developed for 2D cases in MATLAB, which enables quick code development and gives compact and clear code. The speed advantage of the 2D models were

deemed to outweigh the gain in realism of 3D models for the simulation experiments.

After a pre-investigation (ref.[11]) and a pre-study (ref.[12]), the pilot point method proposed by LaVenue and RamaRao (ref.[3],[15]) was found to have the greatest potential for development and was selected as the first candidate. The main difference to their system, as we understand it, is that the LaVenue simulator has a built-in scheme for sequential selection of pilot point locations whereas we have stopped at manual positioning. Beside this, we believe that just minor details in the technical implementation differ.

The results obtained in the previous study (ref.[16]) contributed greatly to the understanding of the large uncertainties in cases with sparse data. We therefore stressed the use of Monte-Carlo simulation also over the actual "truth field" to be modeled. In particular, it was shown that the conditional simulations do not always give smaller variance than unconditional ones. When data are abundant, such as has been the case in the WIPP case studies (ref.[4], [15]), conditioning tends to give sharper results. Some ideas of how the kriging methodology used in the conditioning could be improved to decrease the uncertainty were also gained.

The aim of the present study is to further develop and verify the simulation tool and to perform a simulation experiment with more but still realistically sparse data, as the case will be for an initial site evaluation.

The results obtained in the present study show less uncertainty than in the preceding study. This is mainly due to a modification of the kriging procedure but also to the use of more data. Still the uncertainty in cases of sparse data is apparent. Significant improvements in the uncertainty will be obtained only as the number of data becomes much larger.

The conclusions of the work to date are:

• A quick 2D simulator for method evaluation and what-if simulation has been developed in MATLAB. Conductivity fields are generated by unconditional simulation, conditional simulation on measured conductivities and calibration on both steady-state head measurements and transient head histories. The fields can also include fracture zones and zones with different mean conductivities. Statistics of conductivity fields and particle travel times are recorded in Monte-Carlo simulations.

• Several kriging procedures are implemented, among others Kriging neighbourhoods. In cases where the expectation of the log-conductivity in the truth field is known the non-bias condition can be omitted, which will make the variance in the conditionally simulated conductivity fields smaller.

• A simulation experiment devised in collaboration with SKB was performed and interpreted.

• Large uncertainties in cases with few data are apparent. The variogram represents essential characteristics of the conductivity field. Thus, even unconditional simulations take account of important information. Significant improvements in variance by further conditioning will be obtained only as the number of data becomes much larger.

2. Mathematical Model

In a transient interference test water is usually pumped at constant flow rate in a borehole or a packed off section of a borehole. The change in head (pressure) with time is recorded in this borehole and in packed off sections in other boreholes as well. The pumping phase is followed by a phase of recovery of about the same length. The duration of the pumping phase is usually some days but may in some cases last for months. The head histories recorded in transient interference tests provide information of the capability of bedrock to conduct and store water. For more information about the test procedure see ref.[13] and [14].
The situation we want to simulate is a long term interference pumping test. Conductivities are assumed known at some locations (obtained from single-hole water injection tests in a specific site investigation). These measurements also provide the spatial variability of the conductivity field in terms of a variogram. This information together with the specific storativity field is to be used for the conditioning and calibration of the conductivity field. In the estimated fields, particles in a hypothetical repository are released under steady state conditions and particle travel times are computed.

2.1 Groundwater Flow Equation

To describe the groundwater flow in fractured rock a stochastic continuum model is used. The flow is modeled by Darcian flow and given by the following equation together with appropriate initial conditions and boundary conditions:

$$S_s(\mathbf{x})\frac{\partial h}{\partial t} = \nabla(c(\mathbf{x})\nabla h) + q(x,t) \qquad (1)$$

$$h(\mathbf{x},0) = h_0(\mathbf{x}) .$$

The initial head field $h_0(\mathbf{x})$ is at steady-state, i.e. it is given by

$$\nabla(c(\mathbf{x})\nabla h_0) = 0.$$

In our study we have used boundary conditions of the form

$$\frac{\partial h}{\partial n} = \alpha(\mathbf{x})(h(\mathbf{x},t) - h_{ext}(\mathbf{x},t)).$$

Note that $\alpha = 0$ gives the no-flow boundary condition, and that a very large α gives a prescribed h at the boundary.

The notation used is as follows:

$h(\mathbf{x},t)$	hydraulic head [L]
$S_s(\mathbf{x})$	specific storativity [L^{-1}]
$c(\mathbf{x})$	hydraulic conductivity [LT^{-1}]
$q(\mathbf{x},t)$	pumping source [T^{-1}]
$\alpha(\mathbf{x},t)$	convection coefficient [L^{-1}]
$h_{ext}(\mathbf{x},t)$	external head [L]
n	outward normal at boundary [L].

2.2 Variogram

The standard way of describing the spatial variability in the conductivity field in fractured rock is in terms of a variogram fitted to measurements. In our study we assume intrinsic and isotropic conditions and use for the covariance function C(r) of the log-conductivity either a spherical model

$$C(r) = \begin{cases} V\left(1 - \frac{3}{2}\frac{r}{a} + \frac{1}{2}\left(\frac{r}{a}\right)^3\right) & 0 \le r \le a \\ 0 & r > a \end{cases} \qquad (2)$$

or an exponential model

$$C(r) = Ve^{-\frac{r}{a}},\ r \ge 0. \qquad (3)$$

Here V denotes the variance or sill, r is the norm of the lag vector and a is the range parameter.

3. Solution technique

3.1 Discretization

The domain of computation is a (horizontal) 2D rectangular section, which is discretized by central differences. In each coordinate direction the grid size is constant. Denoting the vector of heads at the nodes by **h** the equation (1) is discretized by spatial finite differences into a system of ordinary differential equations,

$$\mathbf{S}\frac{d\mathbf{h}}{dt} = \mathbf{K}\mathbf{h} + \mathbf{s}(t) \qquad (4)$$

with initial condition

$$\mathbf{h}(0) = \mathbf{h}_0$$

where

h = vector of hydraulic heads
S = storativity matrix (diagonal)
K = conductivity matrix
s(t) = **q**(t) + **b**(t) = vector of source terms.

The source term **s** contains contributions from the boundary **b** as well as the physical sources **q**. The initial field $\mathbf{h}_0$ is computed by solving the steady-state system

$$\mathbf{K}\,\mathbf{h}_0 = -\,\mathbf{b}_0 .$$

For the discretization in time we use the Backward Euler method and arrive at the difference equation

$$\mathbf{A}\mathbf{h}_{n+1} = \mathbf{B}\mathbf{h}_n + \mathbf{s}_{n+1} \qquad (5)$$

with

A = $\mathbf{S}/\Delta t - \mathbf{K}$
B = $\mathbf{S}/\Delta t$
Δt = time step
n = step number.

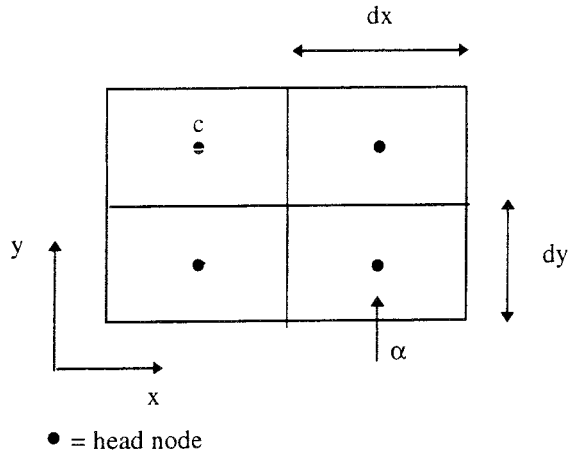

Figure 3.1: Spatial discretization of computational domain

3.2 Simulation of conductivities

In the discussion to follow (3.2, 3.3) we will mainly use **c**, **C** to denote vectors of conductivities and **y**, **Y** for their base 10 logarithms. Capital letters are used for vectors of (^{10}log-)conductivities from the whole discretization while lower case vectors contain measurements and/or pilot point (^{10}log-)conductivities. Further we assume that the log-conductivities obey a normal distribution. The mean of the log-conductivities does not have to be constant in the computational domain. Fracture zones are allowed and defined by a different mean between specified lines. We emphasize that the simulation of (^{10}log-)conductivities, **Y** and **C,** is done at the head nodes (see fig. 3.1) while the conductivity fields **K,** used in the transport equations of sections 3.1 (discretization of the groundwater flow equation) and 3.4 (particle tracking), are represented at the midpoints between head nodes and computed as the geometric mean of the conductivities in the two neighboring head nodes.

3.2.1 Unconditional simulation

An unconditional simulation of a conductivity field produces a pseudo-random field with the same moments (mean and variance) and the same spatial correlation as indicated by the measured conductivities, i.e. obeying the constructed variogram. One possible technique of constructing such a field is the Turning Bands Method (ref.[5]). Another possibility, which is attractive in the 2D case and which we have used, is to use Cholesky factorization of the covariance matrix. This is done as follows (ref.[6]):

1. Compute the covariance matrix **V** of the logarithms of the conductivities in the nodes, evaluated according to the variogram.
2. Compute a lower triangular matrix **L** by Cholesky factorization $\mathbf{V} = \mathbf{L}\mathbf{L}^T$
3. Generate a vector **Z** with independent standard normal components.
4. Compute an unconditional simulation of the log-conductivity field $\mathbf{Y}_{us}$ by

$$\mathbf{Y}_{us} = \mathbf{Y}_{\mu} + \mathbf{L}\mathbf{Z} \qquad (6)$$

where the vector $\mathbf{Y}_{\mu}$ contains the mean field. As mentioned above this mean field is not necessarily constant but can contain a fracture zone with a different mean.

3.2.2 Conditional simulation

A conditional simulation of a conductivity field produces a field, which besides satisfying the requirements for an unconditional simulation, also reproduces the measured values. To create such a field we can modify the unconditional simulation using a procedure involving kriging. Kriging (ref.[7]) is a local estimation technique providing a linear, unbiased estimator which is best in the sense that the variance of the estimator is minimized. It can also be described in terms of a linear interpolation operator since it depends only on structural information; variogram and relative locations of supports (measurements) and estimation points. An estimated field has the property of reproducing the data in the supports. Let $\mathbf{G}_m$ denote the kriging (interpolation) matrix and $\mathbf{y}_m$ the vector of measurements. Then the kriged (interpolated) field $\mathbf{Y}_m$ can be written

$$\mathbf{Y}_m = \mathbf{G}_m \mathbf{y}_m. \qquad (7)$$

Putting the values of the unconditional simulation $\mathbf{Y}_{us}$ (6) in the measurement locations into the vector $\mathbf{u}_m$, another kriged field $\mathbf{U}_m$, now with respect to the simulated field, is obtained

$$\mathbf{U}_m = \mathbf{G}_m \mathbf{u}_m.$$

The differences in the components of

$$\mathbf{Y}_{us} - \mathbf{U}_m = \mathbf{Y}_{us} - \mathbf{G}_m \mathbf{u}_m$$

constitute the kriging errors. As mentioned above these are zero at the locations of measurements and thus by adding them to the field $\mathbf{Y}_m$ (7) we obtain a conditional simulation

$$\mathbf{Y}_{cs} = \mathbf{Y}_m + (\mathbf{Y}_{us} - \mathbf{U}_m) = \mathbf{Y}_{us} + \mathbf{G}_m (\mathbf{y}_m - \mathbf{u}_m) \qquad (8)$$

having the additional property of honoring the measured conductivities.

We make some remarks regarding the kriging. Denote the mean in the unconditionally simulated field by m_{us} and in the truth field, where the measurements are performed, by m_t. Then, interpreting the content of eq. (8) as random functions rather than realizations, we can write the expectation of the conditionally simulated field as

$$E\{\mathbf{Y}_{cs}\} = E\{\mathbf{Y}_{us}\} + \mathbf{G}_m (E\{\mathbf{y}_m\} - E\{\mathbf{u}_m\}) =$$

$$= m_{us}\mathbf{1} + (m_t - m_{us})\,\mathbf{G}_m\mathbf{1}$$

The desired property of the conditionally simulated field is to have the same expectation value as that of the truth field, i.e.

$$E\{\mathbf{Y}_{cs}\} = m_t\mathbf{1} .$$

Combining this with the former equation we get the following condition for the conditional simulation to have the same expectation m_t as that of the truth field

$$(m_{us} - m_t)(\mathbf{1} - \mathbf{G}_m\mathbf{1}) = \mathbf{0} .$$

Two situations can be thought of. If the expectation m_t of the truth field is not known then m_{us} can not be set to make the first factor (m_{us} - m_t) zero and the second factor has to be zero, i.e. the non-bias condition

$$\mathbf{G}_m\,\mathbf{1} = \mathbf{1}$$

has to be imposed. In this case the mean set in the unconditional simulation has no effect at all on the conditional simulation. However if m_t is known then we choose $m_{us} = m_t$ and the non-bias condition can be omitted. In this case the variances in the conditionally simulated fields

will become smaller than or equal to the variances in conditional simulations obeying the non-bias condition (see appendix A). One can also show that they are smaller than or equal to the variances in the unconditionally simulated fields. In our simulation experiments we generate truth fields and compare travel times in unconditioned and conditioned fields. To get a fair comparison between the two one should fully utilize the known mean m_t also in the conditional simulations by omitting the non-bias condition, which is done in the numerical experiment of this study.
In appendix A descriptions of the implemented kriging procedures are given.

3.3 Calibration

The purpose of the calibration is to utilize also steady-state head measurements and transient head histories to improve the realization of the conductivity field. Doing this means that an inverse problem has to be solved. It is well-known that such a problem, i.e. the determination of a conductivity field from measured heads, is ill-posed in general. However it can be made computationally tractable by suitably restricting the high-frequency content in the degrees of freedom of the allowed conductivity field. In the inverse techniques we have chosen, proposed by B.S. RamaRao and A.M. LaVenue (ref.[3]), this is done by letting the log-conductivity in strategically chosen pilot points be the degrees of freedom in the calibration.
Before describing the calibration we give an expression for the calibrated field $\mathbf{Y}_{cc}$ in terms of the output from the calibration; the log-conductivity $\mathbf{y}_p$ in the pilot points. Let $\mathbf{y}_n = (\mathbf{y}_m, \mathbf{y}_p)$ denote the extended vector containing both measurements and computed pilot point values. Similarly, letting $\mathbf{u}_n = (\mathbf{u}_m, \mathbf{u}_p)$ contain the values of the unconditional simulation $\mathbf{Y}_{us}$ in the corresponding locations and $\mathbf{G}_n$ be the kriging matrix, $\mathbf{Y}_{cc}$ can be expressed as a conditional simulation:

$$\mathbf{Y}_{cc} = \mathbf{Y}_n + (\mathbf{Y}_{us} - \mathbf{U}_n) = \mathbf{Y}_{us} + \mathbf{G}_n (\mathbf{y}_n - \mathbf{u}_n) \qquad (9)$$

where

$$\mathbf{Y}_n = \mathbf{G}_n \mathbf{y}_n \text{ and } \mathbf{U}_n = \mathbf{G}_n \mathbf{u}_n.$$

Briefly the calibration means finding the pilot point conductivities that minimize the objective function of head errors for all head-measurement locations and all times. This is done by a conjugate gradient method with

line search, where the gradients are computed by solving the adjoint state equation.

3.3.1 Objective function

The objective function in the calibration is defined by

$$J(\mathbf{y}_p) = \frac{1}{2}\mathbf{e}^T \mathbf{W} \mathbf{e} \qquad (10)$$

where

$$\mathbf{e}^T = (\mathbf{e}_0^T, \mathbf{e}_1^T, ..., \mathbf{e}_{N_t}^T)^T$$

$$\mathbf{e}_j^T = (e_{1j}, e_{2j}, ..., e_{N_m j})^T$$

$\mathbf{y}_p$ = $^{10}\log(\mathbf{c}_p)$ = pilot point ^{10}log-conductivity
e_{ij} = h_{ij} - $h_{meas,ij}$
h_{meas} = measured head
N_m = number of measurements
N_t = number of timesteps
$\mathbf{W}$ = matrix of weights.

In the previous study (ref.[16]), we performed pure transient calibration with the weight 1 for each error e_{ij} corresponding to a diagonal weight matrix of 1's except for the diagonal elements multiplying the initial errors, where there were 0's. In the present study we have generalized the calibration to take also steady-state head measurements of the initial head field into account. The possible options are now three: calibration on transient head histories, calibration on steady-state head measurements and a combination of the two. The latter technique has been used with good results by LaVenue and RamaRao in a case study described in (ref.[4]).
We note that in the steady-state calibration the computational work is reduced since less information is used. Each time integration in the transient calibration (N_t timesteps) is replaced by a single steady-state computation. On the other hand, one would expect to get a better estimation of the true conductivity field in the transient case in view of the richer access to information.

3.3.2 Minimization

For the minimization of the objective function $J(\mathbf{y}_p)$ a conjugate gradient (CG) method by Polak and Ribiere (ref.[8]) is used. In each CG iteration in a search direction $\mathbf{d}_i$ is computed according to

$$\mathbf{d}_i = -\mathbf{g}_i + \beta \mathbf{p}_{i-1}$$

where

$\mathbf{p}_{i-1}$ = search step in CG iteration i–1
$\mathbf{d}_i$ = search direction in CG iteration i
$\mathbf{g}_i$ = gradient of J with respect to $\mathbf{y}_p$

$$\beta = \frac{\mathbf{g}_i^T \mathbf{g}_i}{\mathbf{g}_{i-1}^T \mathbf{g}_{i-1}}$$

and a new estimate $\mathbf{y}_p^{(i)}$ is obtained from

$$\mathbf{y}_p^{(i)} = \mathbf{y}_p^{(i-1)} + \alpha_i \mathbf{d}_i = \mathbf{y}_p^{(i-1)} + \mathbf{p}_i .$$

To estimate α_i , i.e. the steplength in the direction defined by $\mathbf{d}_i$, a line search is performed to find a minimum for J in this direction. This is done by fitting a second order polynomial through three evaluations. The line search is where much of the computational effort lies since every evaluation of J means a time integration of the system (5).

3.3.3 Gradient computation

In each CG iteration the gradient of J with respect to $\mathbf{y}_p$ is needed. To obtain this we start by deriving an expression for the derivatives with respect to the vector $\mathbf{C}$ containing the conductivities at the head nodes. First we will rewrite eq. 5 and for this purpose we split the source term $\mathbf{s}$ in the following way

$$\mathbf{s}_n = \mathbf{q}_n + \mathbf{b}_n = \mathbf{q}_n' + \mathbf{b}_0$$

where

$$\mathbf{q}_n' = \mathbf{q}_n + \mathbf{b}_n - \mathbf{b}_0 .$$

Note that $\mathbf{q_i}$ represents the pumping source and $\mathbf{b_i}$ comes from the boundary conditions. Utilizing the initial condition

$$\mathbf{K}\,\mathbf{h}_0 = -\,\mathbf{b}_0$$

we can now write eq. (5)

$$\mathbf{A}(\mathbf{h}_n - \mathbf{h}_0) = \mathbf{B}(\mathbf{h}_{n-1} - \mathbf{h}_0) + \mathbf{q}'_n \qquad n = 1, \ldots, N_t .$$

These systems form the constraints under which the objective function is minimized and we write them in the form

$$\mathbf{f(C,h)} = \begin{pmatrix} -\mathbf{K}\mathbf{h}_0 - \mathbf{b}_0 \\ \left\{\mathbf{A}(\mathbf{h}_n - \mathbf{h}_0) - \mathbf{B}(\mathbf{h}_{n-1} - \mathbf{h}_0) - \mathbf{q}'_n\right\}_{n=1,N_t} \end{pmatrix} = \qquad (11)$$

$$= \begin{pmatrix} -\mathbf{K} & \mathbf{0} & \mathbf{0} & \ldots & \mathbf{0} \\ \mathbf{0} & \mathbf{A} & \mathbf{0} & \ldots & \mathbf{0} \\ \mathbf{0} & -\mathbf{B} & \mathbf{A} & \ldots & \mathbf{0} \\ \cdot & \cdot & \cdot & \cdot & \cdot \\ \mathbf{0} & \mathbf{0} & . & -\mathbf{B} & \mathbf{A} \end{pmatrix} \cdot \begin{pmatrix} \mathbf{h}_0 \\ \mathbf{h}_1 - \mathbf{h}_0 \\ \mathbf{h}_2 - \mathbf{h}_0 \\ \cdot \\ \mathbf{h}_{N_t} - \mathbf{h}_0 \end{pmatrix} - \begin{pmatrix} \mathbf{b}_0 \\ \mathbf{q}'_1 \\ \mathbf{q}'_2 \\ \cdot \\ \mathbf{q}'_{N_t} \end{pmatrix} = \mathbf{D}\underline{\mathbf{h}} - \underline{\mathbf{q}} = \mathbf{0}$$

where the matrix **D** and "super"vectors $\underline{\mathbf{h}}$ and $\underline{\mathbf{q}}$ have been defined. By defining $\underline{\mathbf{h}}$ in this way we have succeeded in splitting the constraints into a steady-state part and a transient part since **D** consists of two diagonal blocks with zeroes outside. To fully utilize this feature it turns out that it is convenient to introduce new variables for the errors. Let $\underline{\mathbf{h}}_m$ be defined in a similar way as $\underline{\mathbf{h}}$

$$\mathbf{h}_m^T = (\mathbf{h}_0^{mT}, \Delta\mathbf{h}_1^{mT}, \ldots, \Delta\mathbf{h}_{N_t}^{mT})^T$$

where

$$\mathbf{h}_j^{mT} = (h_{1j}^{mT}, h_{2j}^{mT}, \ldots, h_{N_m j}^{mT})^T$$

$$\Delta h_{ij}^m = h_{ij}^m - h_{i0}^m$$

$$h_{ij}^m = h_{meas,ij} .$$

Then the new error $\underline{\mathbf{e}}'$ is given by

$$\underline{\mathbf{e}}' = \mathbf{P}\underline{\mathbf{h}} - \underline{\mathbf{h}}_m$$

where **P** is the matrix selecting the head measurement nodes out of the head nodes. The relation between $\underline{\mathbf{e}}'$ and $\underline{\mathbf{e}}$ is now

$$\underline{\mathbf{e}}' = \begin{pmatrix} \mathbf{I} & \mathbf{0} & \mathbf{0} & \dots & \mathbf{0} \\ -\mathbf{I} & \mathbf{I} & \mathbf{0} & \dots & \mathbf{0} \\ -\mathbf{I} & \mathbf{0} & \mathbf{I} & \dots & \mathbf{0} \\ . & . & . & . & . \\ -\mathbf{I} & \mathbf{0} & \mathbf{0} & . & \mathbf{I} \end{pmatrix} \cdot \underline{\mathbf{e}} = \mathbf{V}\underline{\mathbf{e}} \,. \qquad (12)$$

With this error the objective function takes the form

$$J(\mathbf{y}_p) = \frac{1}{2}\underline{\mathbf{e}}^T\mathbf{W}\underline{\mathbf{e}} = \frac{1}{2}\underline{\mathbf{e}}'^T\mathbf{W}'\underline{\mathbf{e}}'$$

where we choose **W'** as a diagonal matrix diag(γ**I**, **I**, ...,**I**). Thus we consider the errors of $\underline{\mathbf{e}}'$ to be uncorrelated. Here γ can be viewed as a weight factor for the steady-state part of the objective function. Expressed in the original errors $\underline{\mathbf{e}}$ this corresponds to minimization with the weight matrix **W** as

$$\mathbf{W} = \mathbf{V}^T\mathbf{W}'\mathbf{V} = \begin{pmatrix} (\gamma + N_t)\mathbf{I} & -\mathbf{I} & -\mathbf{I} & \dots & -\mathbf{I} \\ -\mathbf{I} & \mathbf{I} & \mathbf{0} & \dots & \mathbf{0} \\ -\mathbf{I} & \mathbf{0} & \mathbf{I} & \dots & \mathbf{0} \\ . & . & . & . & . \\ -\mathbf{I} & \mathbf{0} & \mathbf{0} & . & \mathbf{I} \end{pmatrix}.$$

In the following we simplify the notation for the "super"vectors and use **h**, **e** and **q** instead of $\underline{\mathbf{h}}$, $\underline{\mathbf{e}}$ and $\underline{\mathbf{q}}$. Now the gradient dJ/d**C** can be expressed thus

$$\frac{dJ}{d\mathbf{C}} = \frac{\partial J}{\partial \mathbf{C}} + \frac{\partial J}{\partial \mathbf{h}} \cdot \frac{\partial \mathbf{h}}{\partial \mathbf{C}} = \frac{\partial J}{\partial \mathbf{C}} - \frac{\partial J}{\partial \mathbf{h}} \cdot \left(\frac{\partial \mathbf{f}}{\partial \mathbf{h}}\right)^{-1} \frac{\partial \mathbf{f}}{\partial \mathbf{C}} \qquad (13)$$

since from **f**(**C**,**h**) = **0** (11) we have

$$\frac{\partial \mathbf{f}}{\partial \mathbf{C}} + \frac{\partial \mathbf{f}}{\partial \mathbf{h}} \cdot \frac{\partial \mathbf{h}}{\partial \mathbf{C}} = \mathbf{0} \text{ or } \frac{\partial \mathbf{h}}{\partial \mathbf{C}} = -\left(\frac{\partial \mathbf{f}}{\partial \mathbf{h}}\right)^{-1} \frac{\partial \mathbf{f}}{\partial \mathbf{C}}.$$

The first term $\partial J/\partial \mathbf{C}$ on the right hand side of (13) is zero because the error functional does not depend explicitly on the conductivities. The second term, however, looks quite unpleasant and this is where the adjoint state solution simplifies matters. Introduce the adjoint state λ as the product of the first two factors through

$$\lambda^T = -\frac{\partial J}{\partial \mathbf{h}} \cdot \left(\frac{\partial \mathbf{f}}{\partial \mathbf{h}} \right)^{-1} . \tag{14}$$

By doing this product first we simply apply the analogy of the rule from linear algebra, which states that it is computationally more efficient to perform vector by matrix multiplication before matrix by matrix multiplication. From (11) we deduce $\partial \mathbf{f}/\partial \mathbf{h} = \mathbf{D}$ and thus

$$\mathbf{D}^T \lambda + \left(\frac{\partial J}{\partial \mathbf{h}} \right)^T = \mathbf{0}$$

or equivalently

$$\begin{aligned} -\mathbf{K}\lambda_0 + \left(\frac{\partial J}{\partial \mathbf{h}_0} \right)^T &= \mathbf{0} \\ \mathbf{A}\lambda_n - \mathbf{B}\lambda_{n+1} + \left(\frac{\partial J}{\partial (\mathbf{h}_n - \mathbf{h}_0)} \right)^T &= \mathbf{0} \quad , n = N_t, \ldots, 1 \end{aligned} \tag{15}$$

which are the adjoint state equations we solve, with the condition $\lambda_i = \mathbf{0}$ at $i = N_t + 1$. The source term $(\partial J/\partial \mathbf{h})^T = (\mathbf{W'e'})^T$ contains the errors. Since the last factor in (13) can be expressed as

$$\frac{\partial \mathbf{f}}{\partial \mathbf{C}} = -\frac{\partial}{\partial \mathbf{C}} \begin{pmatrix} \mathbf{K}\mathbf{h}_0 \\ \{ \mathbf{K}(\mathbf{h}_n - \mathbf{h}_0) \}_{n=1,N_t} \end{pmatrix}$$

where $\mathbf{K}$ is the conductivity matrix, the gradient becomes

$$\frac{dJ}{d\mathbf{C}} = \lambda^T \frac{\partial \mathbf{f}}{\partial \mathbf{C}} = \sum_{n=0}^{N_t} \lambda_n^T \frac{\partial \mathbf{f}_n}{\partial \mathbf{C}} =$$

$$= -\lambda_0^T \frac{\partial}{\partial \mathbf{C}}(\mathbf{K}\mathbf{h}_0) - \sum_{n=1}^{N_t} \lambda_n^T \frac{\partial}{\partial \mathbf{C}}(\mathbf{K}(\mathbf{h}_n - \mathbf{h}_0)) \qquad (16)$$

Finally we have to find a transformation to a gradient with respect to $\mathbf{y}_p$. From formula (9) we have

$$\mathbf{Y}_n = \mathbf{G}_n \mathbf{y}_n = \begin{bmatrix} \mathbf{G}_m & \mathbf{G}_p \end{bmatrix} \begin{bmatrix} \mathbf{y}_m \\ \mathbf{y}_p \end{bmatrix} = \mathbf{G}_m \mathbf{y}_m + \mathbf{G}_p \mathbf{y}_p .$$

Applying the chain rule gives

$$\frac{dJ}{d\mathbf{y}_p} = \frac{dJ}{d\mathbf{C}} \cdot \mathrm{diag}(\mathbf{C}) \cdot \mathbf{G}_p \cdot \ln(10) \qquad (17)$$

which together with formula (16) defines the gradient.

3.4 Particle tracking

In the steady-state fields described by the simulated conductivity fields and the given boundary conditions, particle traces are computed. The particles are released from a region and their travel times to the boundary (breakthrough times) are recorded. Introducing $\mathbf{r}(t)$ for the location of a particle at time t initially at $\mathbf{r}(0)$, and $\mathbf{v}(\mathbf{x})$ for the pore velocity at $\mathbf{x}$, the trace is described by the streamline equation

$$\frac{d\mathbf{r}}{dt} = \mathbf{v}(\mathbf{r}) . \qquad (18)$$

The solution is done in two steps:

1. Solve the steady state version of equation (5) (no pumping) for the head field h and use central differences to compute an approximation to the Darcy velocity field $\mathbf{V}(\mathbf{x}) = -c(\mathbf{x})$ grad h in the nodes. Then divide by the porosity to obtain the pore velocity field $\mathbf{v}(\mathbf{x})$.

2. Integrate the stream line equation (18). In our study we have used the Euler method and evaluated the right hand side using bilinear interpolation in each grid block.

4. Computer implementation

4.1 Flowchart

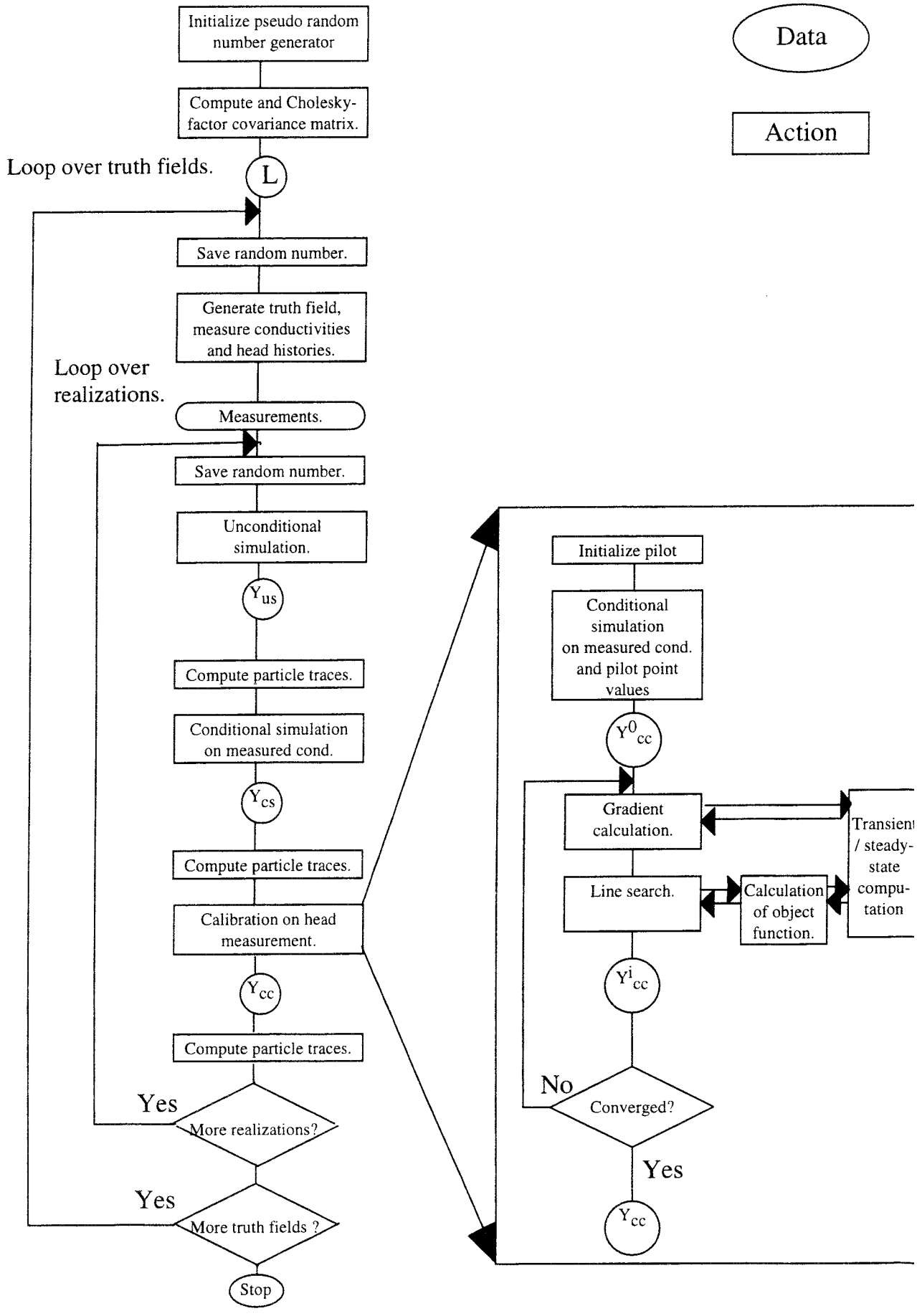

4.2 MATLAB

The implementation is done in the Numeric Computation and Visualization Software package MATLAB (ref[9]). The motivation for using MATLAB is that it supplies high level functions for most operations in linear algebra and provides excellent graphical facilities, which make the development of the code fast and keep the code size small.
The code is divided into a computational part and a problem specification. The specification file is a MATLAB Mfile which contains information about geometry, discretization, boundary conditions, variogram, position of measurements etc.. An example of the problem specification file is shown in appendix C.

4.3 Verification experiment

In the study reported in SKB AR 94-01 (ref.[12]) and SKB AR 94-39 (ref.[16]), many of the routines in our present code were developed. These studies also contained simulation experiments, in 1D and 2D, which exercised and verified the code. The main developments in this study are the introduction of new options of kriging, implementation of fracture zone and the extension of the calibration also to utilize steady-state head measurements. We will here show a verification example, where the steady-state calibration is tested.

4.3.1 Deterministic verification of steady-state calibration

The purpose of this experiment is to verify that the calibration works also on steady-state head measurements. A case with known solution is constructed by letting the initial guess be the unconditionally simulated truth field plus a kriged field given by perturbations in the pilot points. Thus the truth field can actually be obtained by proper choice of the pilot point values. The reduction of the pilot point errors and the decrease in the value of the objective function are shown for two realizations in figures 4.1 and 4.2. These realizations are the same as those used in the corresponding verification of the calibration on transient head histories (ref.[16], figures 4.3 and 4.4). The case presented in figure 4.1 show the same rapid convergence as in the transient calibration. In the other case, figure 4.2, there is convergence not to the global minimum but rather a local minimum of the objective function. Note that in a realistic case the calibration cannot reproduce the truth field and one cannot distinguish global minima from local ones.

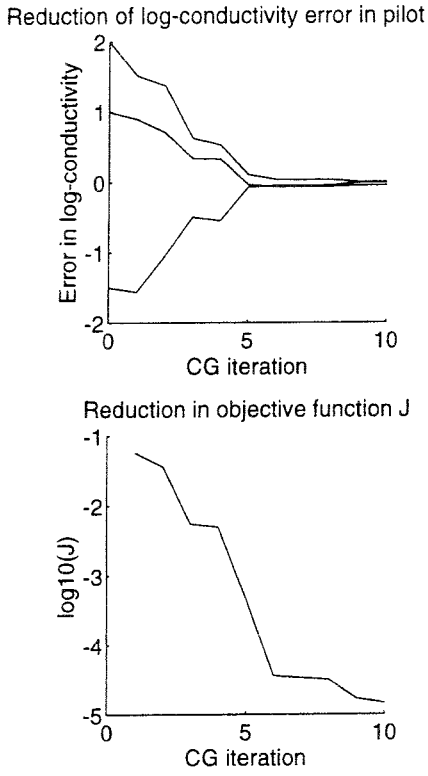

Figure 4.1: Reduction of log-conductivity error in pilot points (above) and reduction in objective function J (below)

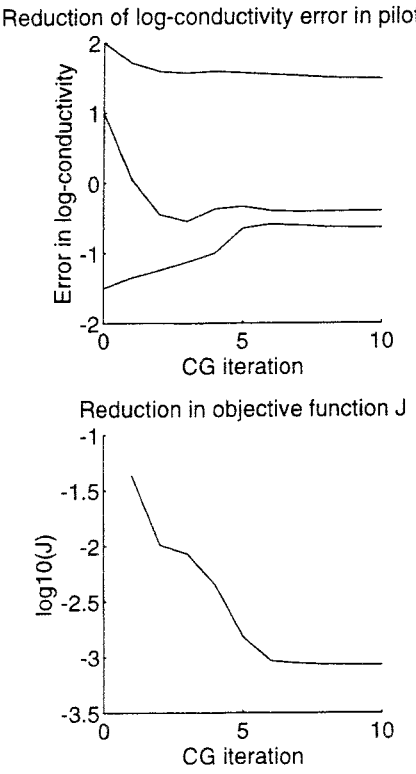

Figure 4.2: Reduction of log-conductivity error in pilot points (above) and reduction in objective function J (below)

4.4 Comparison with pilot point technique by RamaRao & LaVenue

In our implementation the location of the pilot points are chosen manually, where we believe they have the largest potential of influencing the calibration. The incremental technique by LaVenue and RamaRao, on the other hand, has a built-in scheme for sequential selection of pilot point locations. After convergence of the CG iterations new pilot points are selected based on the absolute value of the sensitivity coefficients dJ/d**Y** (see section 3.3.3). Those with the largest absolute value, i.e. with the largest potential of decreasing the value of the objective function, are selected. The old pilot points are then treated as conductivity measurements, i.e. their computed values are fixed.
To get some indications on whether the locations of the pilot points are critical in the calibration a comparison of the two procedures was done.
This was done by performing a sequence of calibrations, where new pilot points were selected manually based on sensitivity coefficients and old ones were treated as measurements. All 21x31 gridpoints were considered candidates.
The manual procedure involved made us limit the comparison to one realization. We choose to look at one realization of case 1 of the numerical experiment in our previous report (ref.[16]) and as a measure of how the calibration succeeds we used the reduction in the objective function.
In figure 4.3 the computational domain with conductivity measurement locations (x) and their ranges (circles) are shown. The pumping source coincides with the conductivity measurement at the middle of the domain and the head histories are recorded at the three closest measurement locations.
In the transient calibration based on our technique we used 12 manually positioned pilot points, marked (+) in figure 4.3, and allowed 20 CG-iterations. The reduction in the logarithm of the objective function J as a function of iteration number is shown in the figure 4.3.
The calibration based on the technique by RamaRao and LaVenue is illustrated in figure 4.4. To reproduce their technique we performed a sequence of four calibrations with different sets of pilot points. In the first calibration the three pilot points marked (+) were used since the absolute value of the sensitivity coefficients dJ/d**Y** were largest at these locations in the field conditioned on the conductivity measurements. After five CG-iterations three new pilot points (*) were chosen in a similar way in the calibrated field and in the following calibration the old pilot points with their computed conductivities were treated as conductivity measurements. In all, four calibrations were performed with

four sets of pilot points (+, *, o, .) yielding a total of 12 pilot points and 20 CG-iterations, i.e. the same numbers as were used in the simulation based on our implemented technique. At the bottom of figure 4.4 the reduction in the objective function is shown.
The improvement when new pilot points are added is clearly seen as jumps at 5 and 10 iterations. The last group has little effect. In this case the initial manual selection did better than the sequential. We note that the sequential algorithm clusters pilot points around measurement points. Thus, the grid of candidate points has a strong influence since it determines the minimum separation between pilot points.

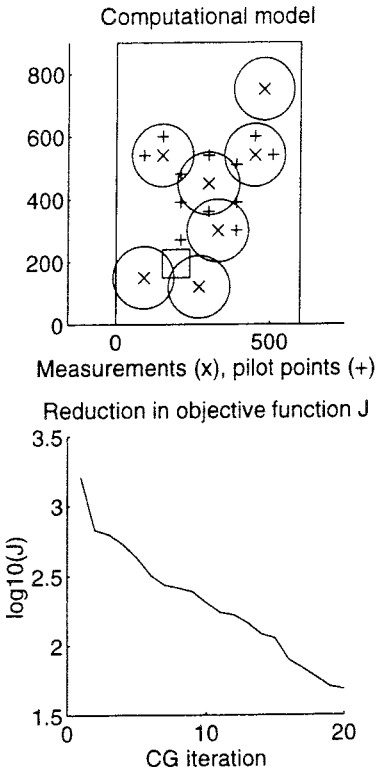

Figure 4.3: Computational domain with conductivity measurements (x) and pilot points (+) (above) and reduction in objective function J (below)

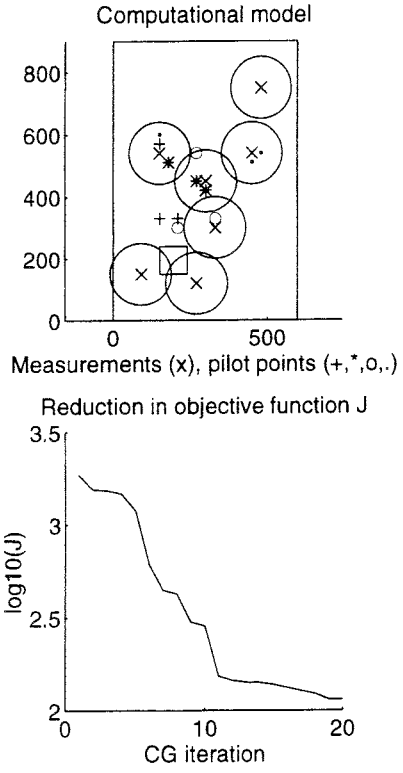

Figure 4.4: Computational domain with conductivity measurements (x) and pilot points (+, *, o, .) (above) and reduction in objective function J (below)

5. Simulation experiment

A simulation experiment has been performed to estimate the particle travel times from a repository to a given boundary. The computational model for the experiment was designed in cooperation with SKB to resemble a typical model in initial stages of a site investigation. The domain of computation is the same as in the numerical experiment performed in the previous study (ref.[16]) but modified in accordance with the experience from that study. It was decided to include more data, both conductivity measurements and head measurements, but within the frames of what is realistic in an initial site evaluation. In that study we also observed large differences in the results obtained for substantially different truth fields. Therefore we wanted to use a more representative set of truth fields. They were chosen to be approximately "normally" distributed with respect to the mean log-conductivity in an area covering the repository and a portion of the domain where the particles are most likely to travel.

The simulation experiment is specified as follows:

* Define 2D model (fig. 5.2) with
  - boundary conditions,
  - repository,
  - boreholes with
    - conductivity measurements,
    - head measurements,
    - pumping history,
  - conductivity variogram.
* Define result as
  - particle log(travel time) from repository to boundary of computational model.
* Define answer as
  - mean log(travel time) in ensemble of Monte Carlo simulations.
* Define accuracy/quality as
  - log(travel time) variance.

In our experiment we have 13 measurements of conductivity, which is very few compared to e.g. the WIPP site (ref.[4]) with conductivity measurements in 41 wells. Few measurements means large uncertainties in the truth field and therefore Monte Carlo simulations are performed also over the truth fields. Note that the answer was chosen to be

log(travel time) and not travel time, as in the previous study. Presenting the results in log(time) is more natural in view of the conductivities being log-normally distributed.

The numerical experiment is carried out as follows:

Do M times
    Choose as the truth a realization respecting the variogram.
    Generate simulated measurements from truth field for the conditioning.
    Do N times
        Make a realization $\mathbf{Y}_{us}$ respecting the variogram.
        Record particle breakthrough times.

        Make a realization $\mathbf{Y}_{cs}$, based on $\mathbf{Y}_{us}$ and conditioned on the conductivities only.
        Record particle breakthrough times.

        Make a realization $\mathbf{Y}_{cc}$, based on $\mathbf{Y}_{us}$ and conditioned on the conductivities and head histories and/or steady-state head measurements.
        Record particle breakthrough times.

In the experiment we had M = 6 and N = 100. We make some remarks on the experiment.

1. The six truth fields are chosen out of a set of 100 unconditionally simulated realizations of the log-conductivity field. The criteria for the selection are two. Firstly they have to have different mean log-conductivity in an area covering the repository and a portion of the domain where the particles are most likely to travel. Six fields with this mean "normally" distributed around the expectation are selected. Truth field 1 is assigned the field with the lowest mean, truth field 2 the next to the lowest etc.. These fields also satisfy the second criterion, which is that the mean of the 13 log-conductivity measurements be close to the expectation.

2. The locations of pilot points are chosen manually (see fig.5.2).

3. In the kriging procedure the non-bias condition is omitted. This will make the variances in the conditional simulations smaller.

4. The boundary conditions, which are of Dirichlet type and chosen to give an average flow towards the upper boundary of fig.5.2, are part of the computational model. As such they have a strong influence on the flow, which may seem unsatisfactory. In site modelling the boundary conditions should be considered uncertain as well as the conductivity field. Calibration with respect to boundary conditions could also be performed, but is excluded in the present study.

4. For each realization travel times are saved for the 25 particles, starting from the 25 grid points of the deposit. Random number seeds are also saved to enable re-runs of individual realizations.

For case 1 we show several statistics:

- Particle trace of particle 5 in truth field (fig. 5.3).
- Particle traces of particle 5 in the 100 unconditionally simulated fields (fig. 5.4).
- Particle traces of particle 5 in the 100 conditionally simulated fields (fig. 5.5).
- Particle traces of particle 5 in the 100 transient calibrated fields (fig. 5.6).

For cases 1, 4 and 6 we show:

- Six histograms with log(breakthrough times) for two particles, 5 and 21, with no conditioning, with conditioning on measured conductivities and with transient calibrated conductivities (fig. 5.7 to 5.9).

The following data were used in the simulation experiment .

h prescribed on the boundary, $\alpha = 100$, (see fig. 5.2),
and

$<K> = 10^{-9}$ m/s
$S_S = 10^{-7}$ m^{-1}
$q(\mathbf{x},t)$ = point source $q(t)$ at $\mathbf{x}_q$ (location $\mathbf{x}_q$ see fig. 5.2)

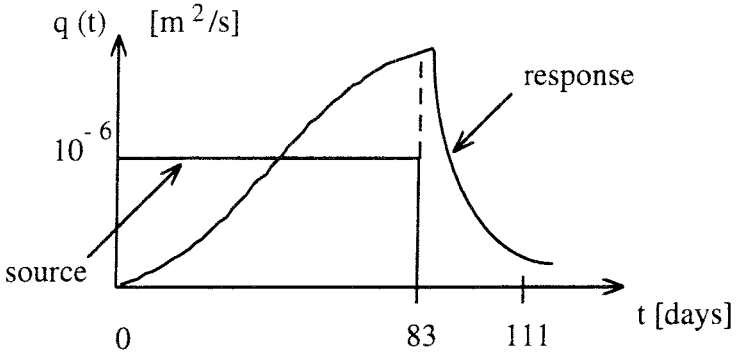

Figure 5.1: Flow rates in pumping test

Spherical variogram for $^{10}\log$ (K),
variance = 1, range = 100 m.

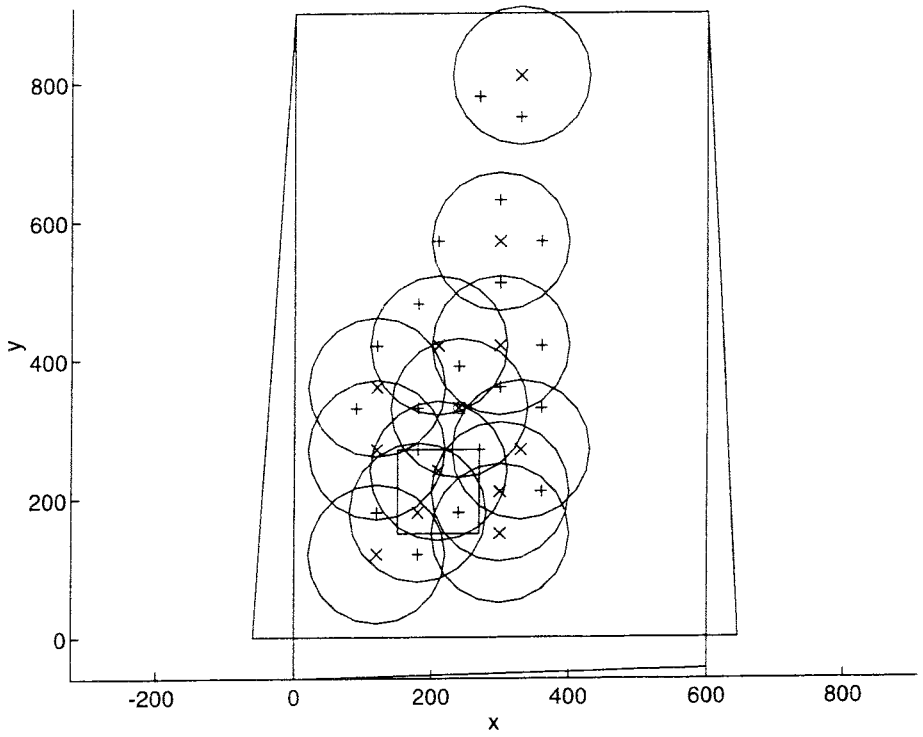

Figure 5.2: Computational model with conductivity measurements (x) and ranges, head measurements (x), pilot points (+) and pumping source (o). The external head varies linearly along the boundaries as indicated and is 2 at (0,0), 1.5 at (600,0) and 0 at (0,900) and (600,900). The repository is indicated by the square.

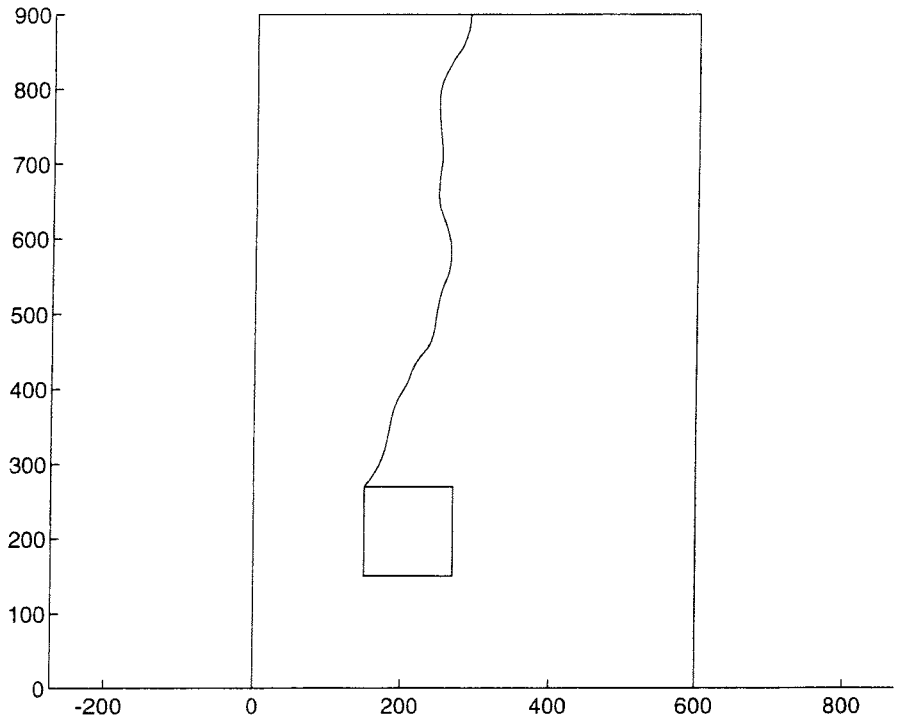

Figure 5.3: Trace of particle 5 in truth field 1

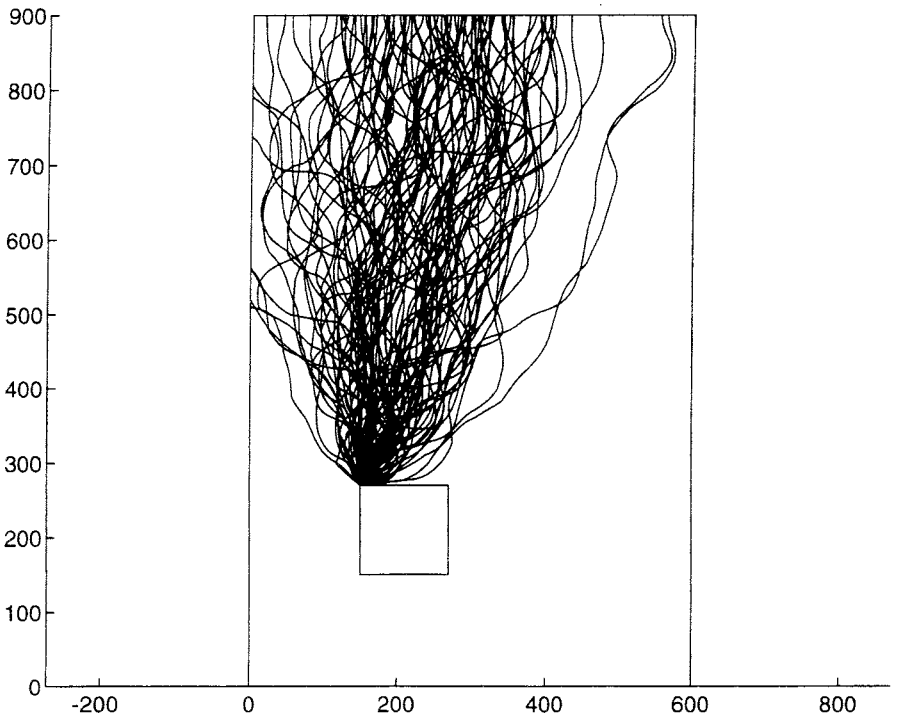

Figure 5.4: Traces of particle 5 in the unconditional simulations, case 1

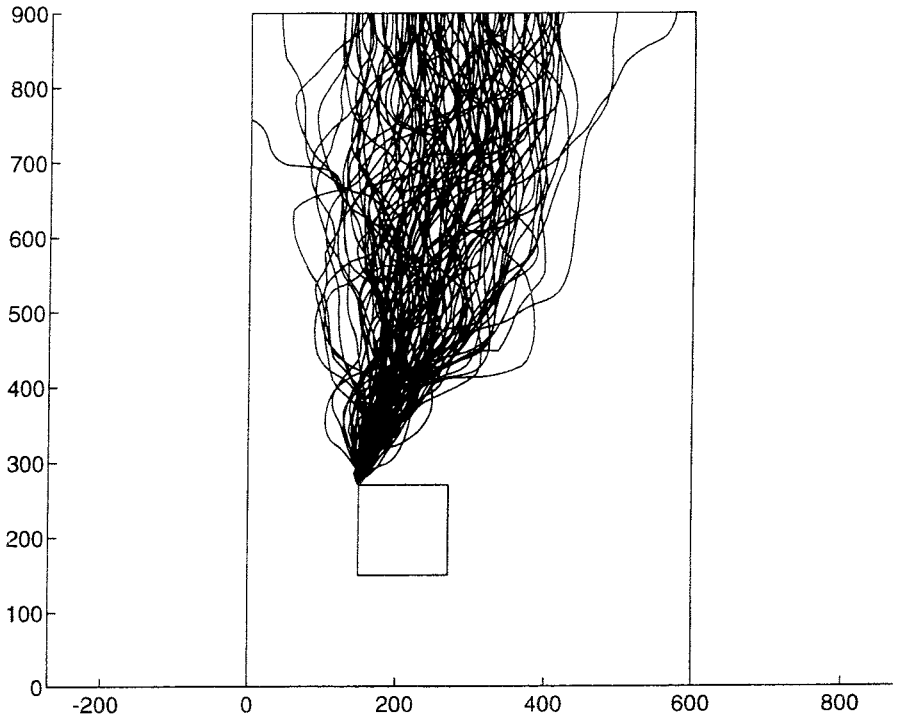

Figure 5.5: Traces of particle 5 in the fields conditioned on conductivities, case 1

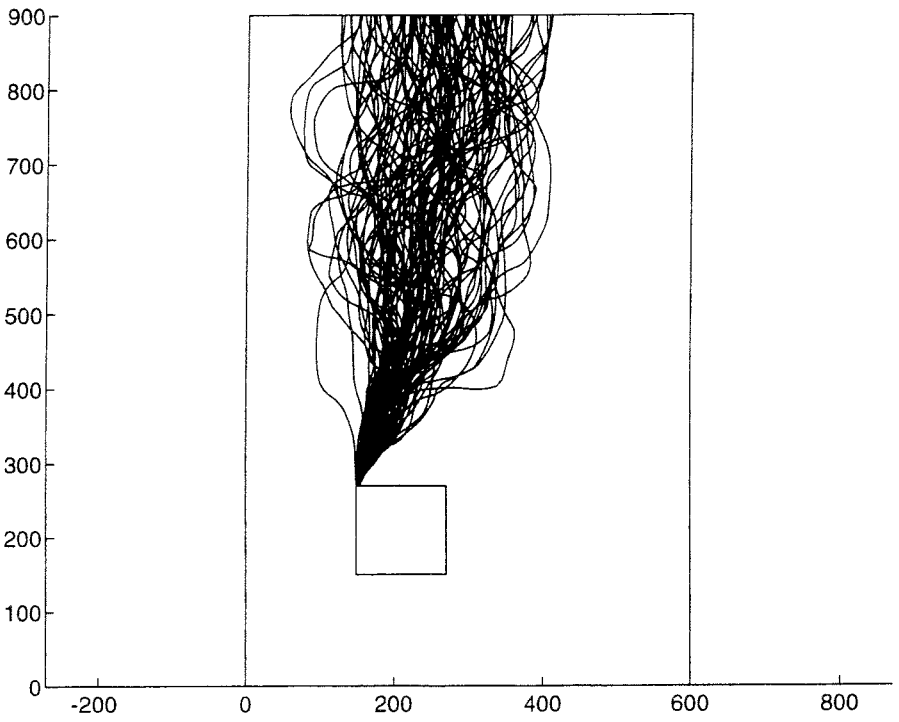

Figure 5.6: Traces of particle 5 in the transient calibrated fields, case 1

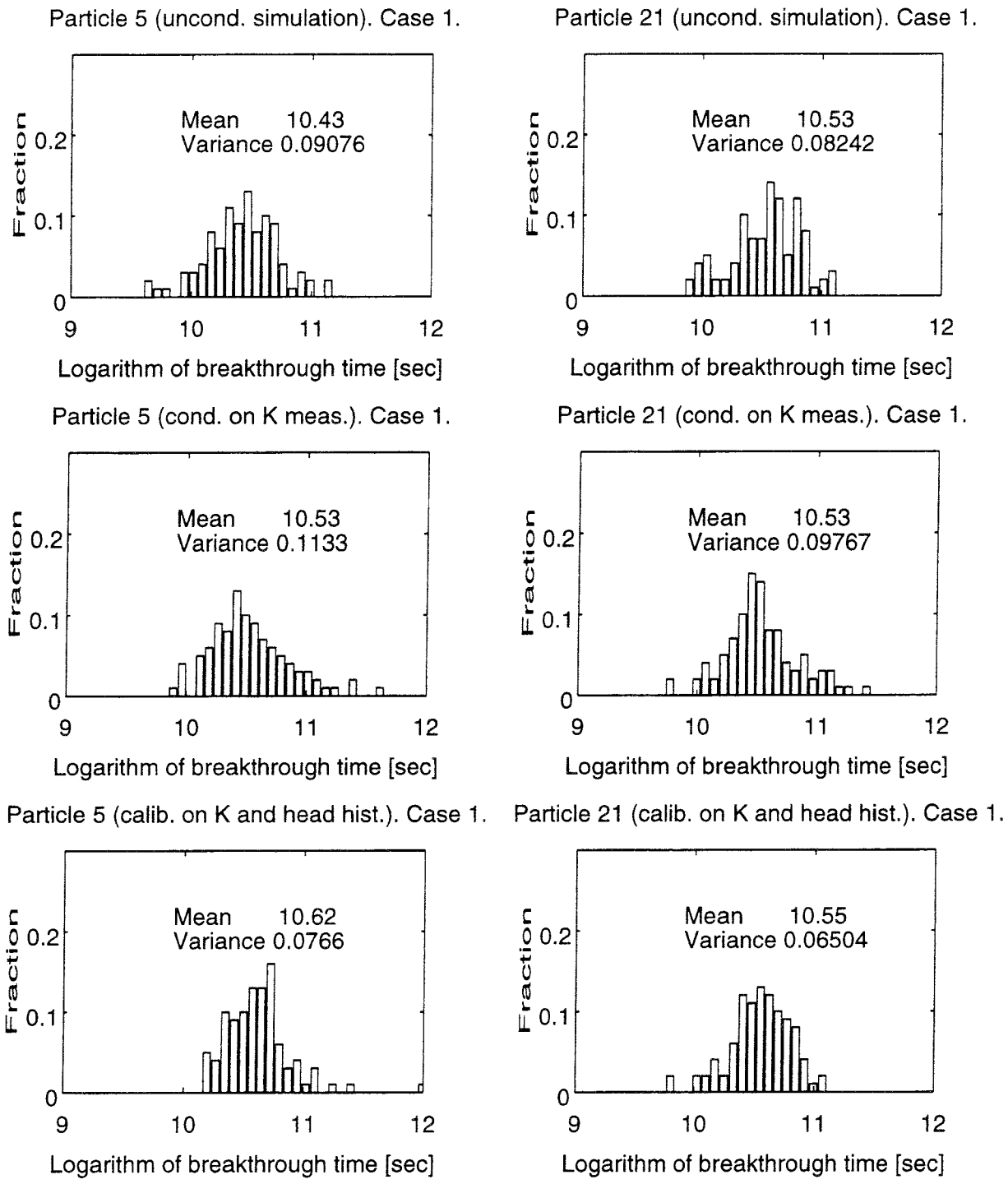

Figure 5.7: Histograms showing log(breakthrough time) for particles 5 (left) and 21 (right), without conditioning (top), with conditioning on measured conductivities (middle) and with calibrated conductivities (bottom) for case 1

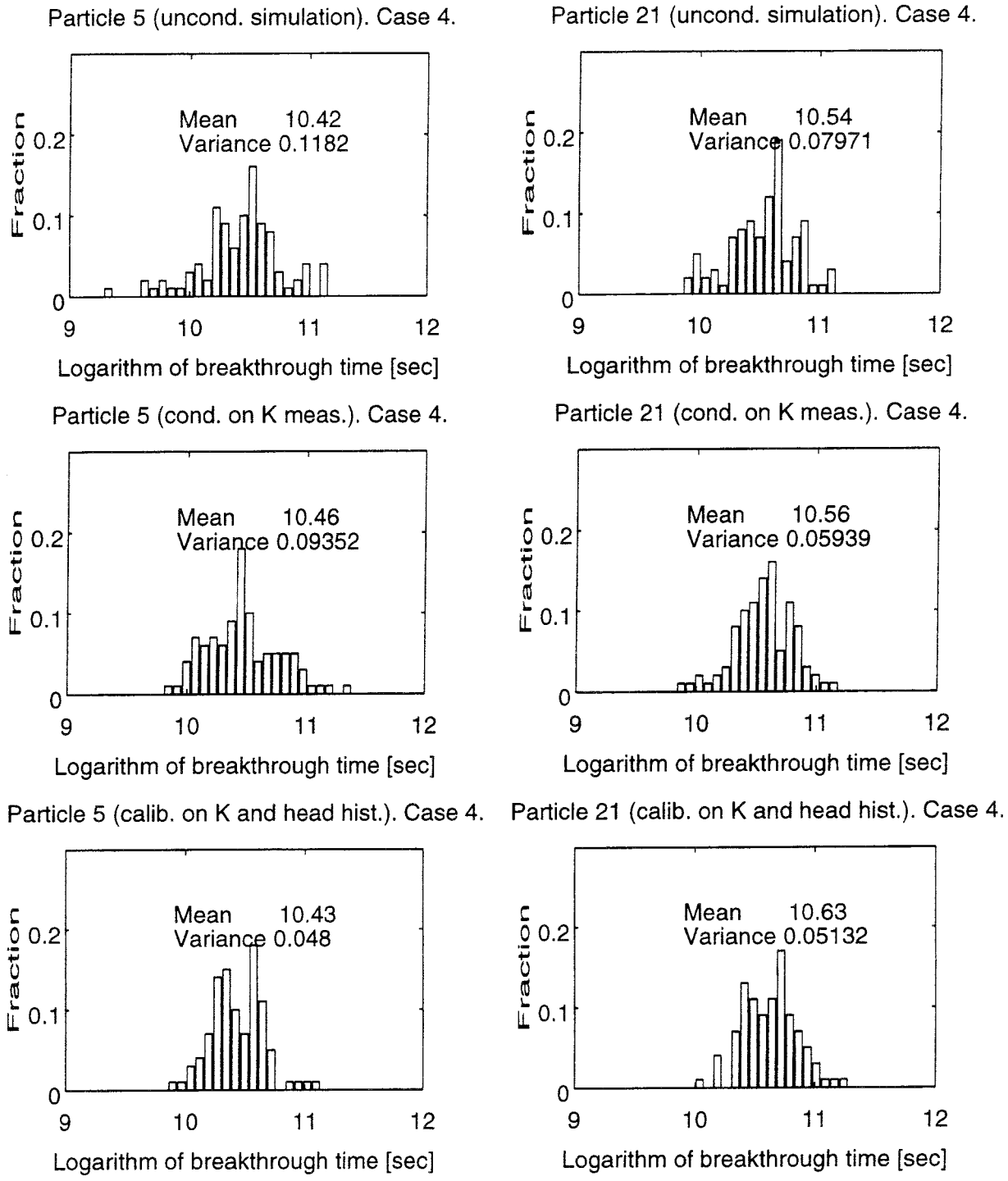

Figure 5.8: Histograms showing log(breakthrough time) for particles 5 (left) and 21 (right), without conditioning (top), with conditioning on measured conductivities (middle) and with calibrated conductivities (bottom) for case 4

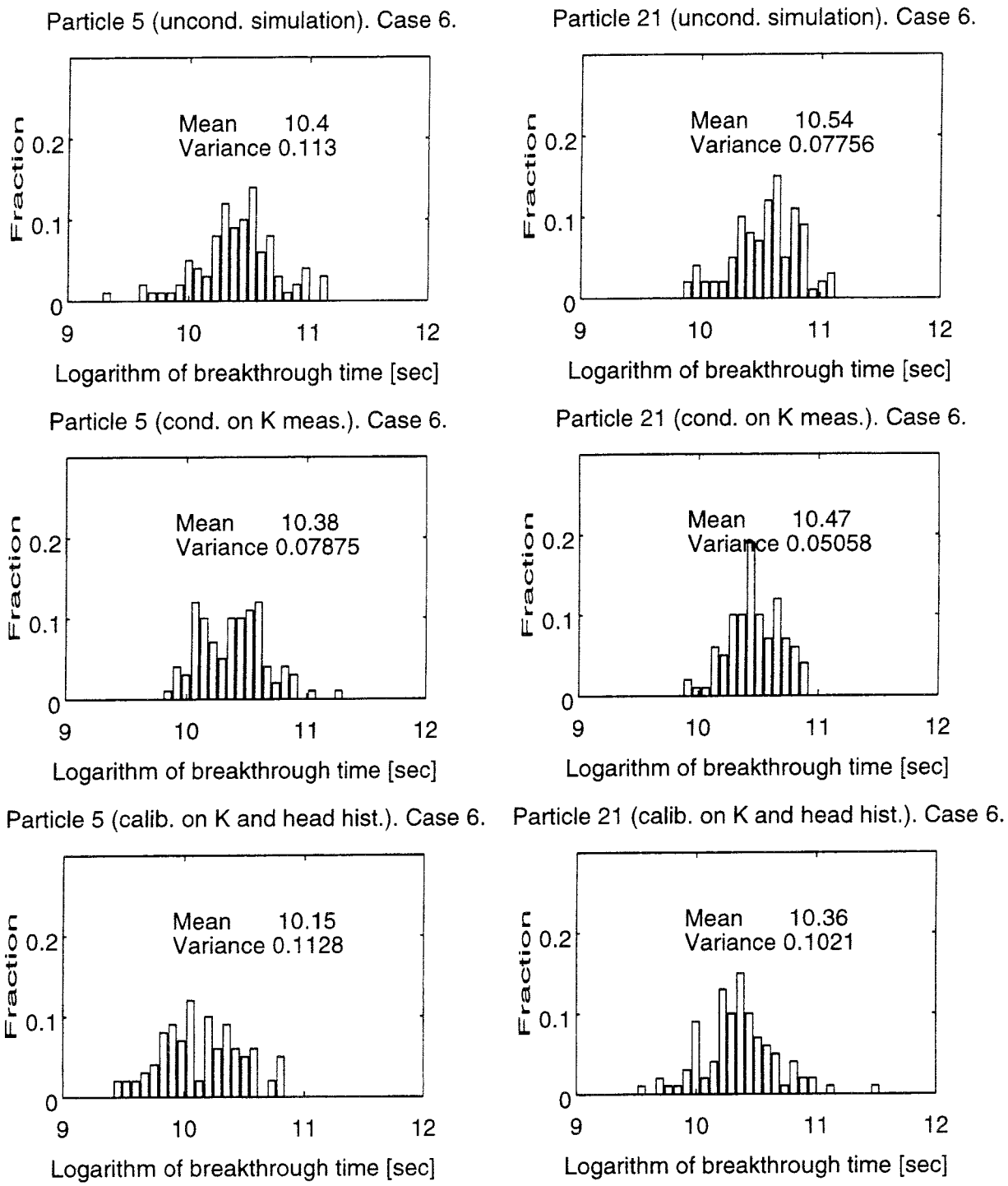

Figure 5.9: Histograms showing log(breakthrough time) for particles 5 (left) and 21 (right), without conditioning (top), with conditioning on measured conductivities (middle) and with calibrated conductivities (bottom) for case 6

6. Results and discussion

6.1 Simulation experiment

The design of the simulation experiment is based on the experiences from our previous study (ref [16]). The results and patterns seen dimly in our earlier study have now taken more definite shape owing to the improvement in Kriging technique and a better designed experiment with more data.
The basic question is the relation between precision of the answer obtained to cost of obtaining the data.
In order of increasing cost (data and computation) the procedures employed are

Name	**Data used**
U	Variogram
C	U + K-measurements
S	C + steady H-data
T	C + transient H-data

In figure 5.10 we have summarized the travel time statistics of the numerical experiment. For U, C, S, and T of each of the six truth cases, the mean of the particle mean and variance (of log(travel time)) is displayed in terms of confidence intervals ($\pm 2\sigma$). As a reference, the mean in the truth field (E) is also displayed.
The most striking feature is that variance differences overall are small: The U-variance is hardly significantly larger than the T-variance. The interpretation is as follows: all procedures use the same variogram, which in practice is obtained from the same borehole data as used for the conditioning. It appears that this is the most important datum; the unconditional simulations really use a lot of the data in the form of the variogram.
It is also seen that the more costly procedures give improved means in the cases where the U-mean deviates much from the correct, better the more data is used, an improvement not seen in the variance.
We venture the following conjecture: The variance will be proportional to 1/N if N is a representative number for the amount of data used. This is a law of diminishing return for investment in data acquisition which effectively rules out high precision. Significant improvements in variance will be obtained only as the number of data becomes much larger.

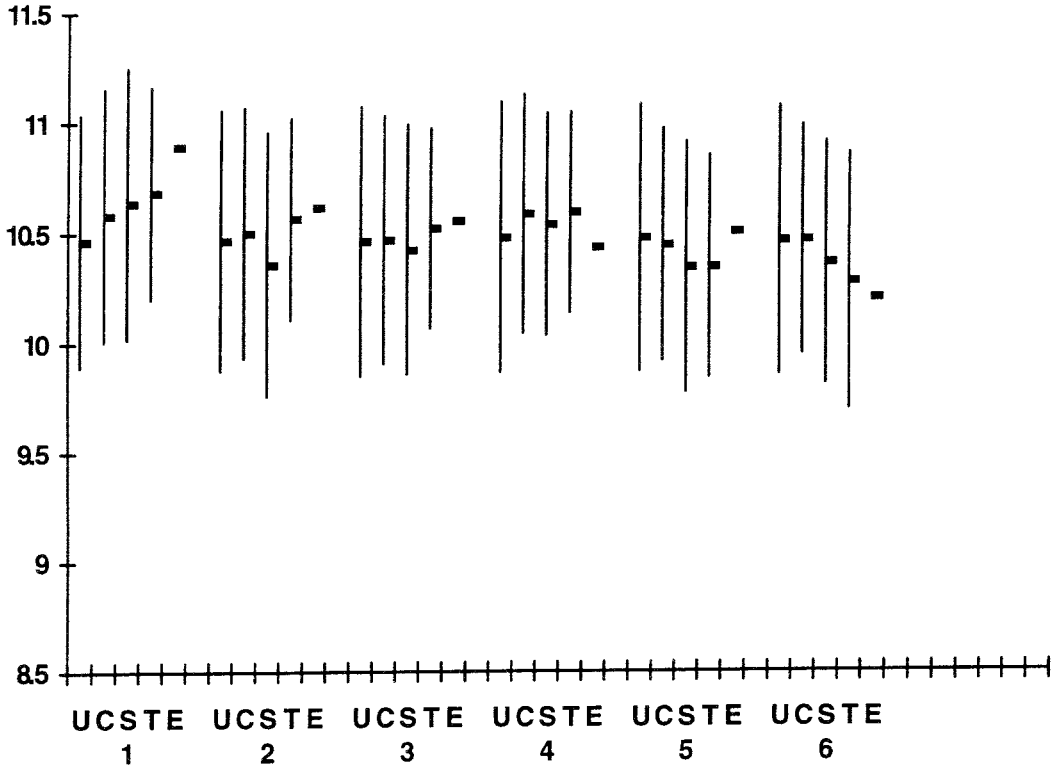

Figure 5.10: Computed means and confidence intervals ($\pm 2\sigma$, where σ is the standard deviation) of the logarithms of particle breakthrough times in the six Monte-Carlo simulations. Notation used is: unconditioned fields (U), fields conditioned on measured conductivities (C), steady-state calibrated fields (S) and transient calibrated fields (T). The means for the truth fields are denoted by (E).

In the following we look in some detail at the results of the simulation experiment.

Particle traces.
Figures 5.3 to 5.6 show particle traces of particle 5 in case 1. In figure 5.3 the path in the truth field is shown. In the following 3 figures, 5.4 and 5.6, the effect of the conditioning on the dispersion of the particle paths in the 100 realizations is demonstrated. The large dispersion in the conditional simulations, fig. 5.4, is decreased by conditioning on measured conductivities, fig. 5.5. In the calibrated fields the ensemble of travel paths is further centered around the true path.

Travel time statistics.
In figures 5.7 to 5.19 histograms of the logarithm of the travel times for two particles are shown. We note that in general conditioning and calibration successively reduce the variance and that the variance always is smallest in the conditioned fields, either calibrated or conditioned on

conductivities. For both particles the mean and variance differ very little in the unconditional simulations between the six cases. This indicates that 100 realizations per truth field is sufficient for the precision required in our numerical experiment.

6.2 Development of simulation tool

The current study has produced a refinement of the simulator developed in our previous study (ref [16]). It allows quick method evaluation and what-if simulations.
The simulator has been developed in MATLAB. Conductivity fields are generated by unconditional simulation, conditional simulation on measured conductivities and calibration on both steady-state head measurements and transient head histories. The fields can also include fracture zones and zones with different mean conductivities. Statistics of conductivity fields and particle travel times are recorded in Monte-Carlo simulations.
Several kriging procedures are implemented, among others Kriging neighbourhoods. In cases where the expectation of the log-conductivity in the truth field is known the non-bias condition can be omitted, which will make the variance in the conditionally simulated conductivity fields smaller.
The results obtained in the present study show less uncertainty than in the preceding study. This is mainly due to a modification of the kriging procedure but also to the use of more data. Still the uncertainty in cases of sparse data is apparent. Significant improvements in the uncertainty will be obtained only as the number of data becomes much larger.
It is now a flexible and useful tool for 2D stochastic continuum simulations of groundwater flow, including inverse modelling techniques.

6.3 Inverse modelling by the Pilot point method

The pilot point method was chosen for its flexibility in implementation and reportedly strong potential for variance reduction. The results of this study support the first statement clearly and do not contradict the second. It is not clear how sensitive the variance reduction is to pilot point locations. The small experiment of section 4.4 showed comparable improvements with the sequential technique by RamaRao and LaVenue and the manual one. The sequential method uses a grid of candidate points which should not be too fine; better results could probably have

been obtained with the sequential method if pilot points had not been allowed to cluster.

7. References

[1] Marsily, G. de, Lavedan, C., Boucher, M., Fasanino, G., *Interpretation of Interference Tests in a Well Field Using Geostatistical Techniques to Fit the Permeability Distribution in a Reservoir Model*, in Geostatistics for Natural Resources Characterization, Second NATO Advanced Study Institute, GEOSTAT 1983, Tahoe City, California, edited by G. Verly, M. David, A.G. Journel, and A. Marechal, pp. 831-849, D. Reidel, Hingham, Mass., 1984.

[2] Carrera, J., Neuman, S.P., *Estimation of Aquifer Parameters Under Transient and Steady State Conditions, 2, Uniqueness, stability, and solution algorithms,* Water Resour. Res., 22(2),211-227, 1986.

[3] RamaRao, B.S., LaVenue, A.M., de Marsily, G., Marietta, M.G., *Pilot Point Methodology for Automated Calibration of an Ensemble of Conditionally Simulated Transmissivity Fields: Part 1 - Theory and Computational Experiments,* private comm., to appear.

[4] LaVenue, A.M., RamaRao, B.S., de Marsily, G., Marietta, M.G., *Pilot Point Methodology for Automated Calibration of an Ensemble of Conditionally Simulated Transmissivity Fields: Part 2 - Application,* private comm., to appear.

[5] Matheron, G., *The Intrinsic Random Functions and their Application,* Adv. Appl. Prob. 5, 439-468, 1973.

[6] Bratley, P., Fox, B.L., Schrage, L.E., *A Guide to Simulation,* Second Edition, Springer-Verlag.

[7] Journel, A.G., Huijbregts,Ch.J., *Mining Geostatistics,* Academic Press,1978.

[8] Numerical Recipes, The Art of Scientific Computing, Cambridge University Press, 1986,1989.

[9] MATLAB ver. 4.0. User's Guide, Reference Guide, The MathWorks Inc., 1992,1993.

[10] Dagan, G., *Solute transport in heterogeneous porous formations,* J. Fluid Mech., 145, 151-177, 1984.

[11] Hörnfeldt, P., Lovius, L., Oppelstrup, J., *Implementing a transient solver and calibration features in HYDRASTAR, a pre- investigation,* SKB AR 93-32.

[12] Oppelstrup, J., Eriksson, L., Hörnfeldt, P., *A Study of Calibration Techniques for the Transient Hydrology Equation using MATLAB,* SKB AR 94-01.

[13] Wikberg, P., Gustafson, G., Rhen, I., Stanfors, R., *Äspö Hard Rock Laboratory. Evaluation and conceptual modelling based on the pre-investigations 1986-1990* , SKB Technical Report TR 91-22.

[14] Rhen, I., *Transient interference tests on Äspö 1988,* SKB HRL PR 25-88-13.

[15] LaVenue, A.M., RamaRao, B.S., *A modeling Approach to Address Spatial Variability within the Culebra Dolomite Transmissivity Field,* Contract Rep. SAND92-7306. Albuquerque, NM: Sandia National Laboratories, 1992.

[16] Eriksson, L.O., Lovius, L., Lindgren, M., Oppelstrup, *Calibration with respect to transient head histories in stochastic simulation of groundwater flow: An SKB pilot project,* SKB AR 94-39.

Appendix A.
Kriging procedures implemented.

We will here describe the kriging procedures implemented in the MATLAB code. For this purpose we first derive theoretical estimations of the variances in conditioned log-conductivity fields.
Denote a row of $\mathbf{G}_m$ (eq. (8)) by λ^T. Then the kriging system (ref[7]) for a point at $\mathbf{x}$ in a conditional simulation obeying the non-bias condition is

$$\begin{bmatrix} \mathbf{K} & \mathbf{1} \\ \mathbf{1}^T & \mathbf{0} \end{bmatrix} \begin{bmatrix} \lambda \\ -\mu \end{bmatrix} = \begin{bmatrix} \mathbf{k} \\ 1 \end{bmatrix} \qquad \text{(A.1)}$$

where

$\mathbf{K}$ = covariance matrix for data supports (measurements)
$\mathbf{k}$ = vector of covariances between current point and data supports
λ = vector of kriging weights
μ = Lagrange parameter.

The bottom partition of the system is the scalar version of the non-bias condition (see section 3.2.2)

$$\mathbf{G}_m \mathbf{1} = \mathbf{1} .$$

The solution λ without and with this condition is

$$\lambda = \begin{cases} \mathbf{K}^{-1}\mathbf{k} & \text{without non-bias condition} \\ \mathbf{K}^{-1}(\mathbf{k}+\mu\mathbf{1}) & \text{with non-bias condition} \end{cases} . \qquad \text{(A.2)}$$

Using eq. (8) of 3.2.2, with content interpreted as random functions rather then realizations, and denoting the variance in the unconditional simulation by $\sigma_{us}^2 = \sigma^2$ the variance in the conditional simulation can be expressed

$$\sigma_{cs}^2 = E\left\{\left[\mathbf{Y}_{cs}(\mathbf{x}) - \mathbf{Y}_m(\mathbf{x})\right]^2\right\} = E\left\{\left[\mathbf{Y}_{us}(\mathbf{x}) - \mathbf{U}_m(\mathbf{x})\right]^2\right\} =$$

$$= E\left\{\left[\mathbf{Y}_{us}(\mathbf{x}) - \lambda^T \mathbf{u}_m\right]^2\right\} =$$

$$= E\left\{\left[\mathbf{Y}_{us}(\mathbf{x})\right]^2\right\} - 2E\left\{\left[\lambda^T \mathbf{u}_m \mathbf{Y}_{us}(\mathbf{x})\right]\right\} + E\left\{\left[\lambda^T \mathbf{u}_m \mathbf{u}_m^T \lambda\right]\right\} =$$

$$= \sigma^2 - 2\lambda^T \mathbf{k} + \lambda^T \mathbf{K} \lambda =$$

$$= \begin{cases} \sigma^2 - \mathbf{k}^T \mathbf{K}^{-1} \mathbf{k} & \text{without non-bias condition} \\ \sigma^2 - \mathbf{k}^T \mathbf{K}^{-1} \mathbf{k} + \mu^2 \mathbf{1}^T \mathbf{K}^{-1} \mathbf{1} & \text{with non-bias condition} \end{cases}$$

Denote the variance in conditional simulations obeying the non-bias condition by σ^2_{csn} and in simulations not obeying the non-bias condition by σ^2_{csb}. Then, since **K** is positive definite, we have

$$\sigma^2_{csb} \leq \sigma^2_{csn}$$

$$\sigma^2_{csb} \leq \sigma^2_{us}$$

i.e. conditional simulations not obeying the non-bias condition yield the smallest variances.
In the previous study (ref[16]) we saw that σ^2_{csn} was larger than σ^2_{us} except in the vicinity of the measurements. This observation suggested the use of kriging neighbourhood as a mean of decreasing the variance.

The following kriging procedures are implemented in the MATLAB code:

1. Kriging with non-bias condition. The kriging weights λ are computed according to eq. 2 of (A.2).
2. Kriging neighbourhood within ranges. The weight vector λ at a location **x** is computed for a local kriging system, of the form (A.1), constructed from the data supports, whose ranges contain the point **x**. Note that for points outside the ranges the weights are zero making the conditional simulation identical to the unconditional simulation there.
3. Kriging neighbourhood where $\sigma^2_{csb} \leq \sigma^2$. At locations where this condition is satisfied the weight vector is computed

according to eq. 2 of (A.2) and set zero otherwise. In this case the neighbourhoods become smaller than in procedure 2 since the condition is satisfied only in parts of the ranges.

4. Kriging without non-bias condition. The kriging weights λ are computed according to eq. 1 of (A.2). We note that also in this case the kriging weights for points outside the ranges become zero, since **k** is a zero vector there.

These procedures of kriging have been tested in Monte-Carlo simulations to estimate travel times. The results indicate that kriging without non-bias condition (procedure 4) gives the smallest variances in log(travel time). This is also what one would expect in view of the theoretical discussion above. The procedures of kriging neighbourhood, especially procedure 3, showed little improvement in variance compared to the unconditional simulations when applied in the numerical experiment of the previous study (ref[16]).

Appendix B.
An example of conditioning on more data.

To illustrate the dependency on the amount of data in the conditioning we show an experiment with more data. The computational model is the same as in the numerical experiment (sec. 5) but instead of 13 conductivity measurements there are 42. The locations of the measurements are shown in fig. B.1. We compare unconditional simulations, denoted by (U), and simulations conditioned on conductivities, denoted by (C).

The comparison includes 11 truth cases, with 100 realizations for each. In figure B.2 we have summarized the travel time statistics of the experiment. For U and C of each of the eleven truth cases, the mean of the particle mean and variance (of log(travel time)) is displayed in terms of confidence intervals ($\pm 2\sigma$). The mean in the truth field (E) is also displayed.

An improvement, somewhat larger in average than in the numerical experiment with 13 measurements, is obtained in all 11 cases but not as big as one intuitively might expect. The conjecture of the numerical experiment is further supported: the unconditional simulations contain a lot of data in the form of the variogram and significant improvements in variance is obtained only as the number of data becomes much larger.

Figure B.3 illustrates the effect on the computed particle traces. The paths of particle 5 in the conditioned fields are displayed for truth case 4, which is identical to truth case 1 of the numerical experiment in section 5. Comparing figure B.3 with figures 5.3-6 a narrowing of the dispersion pattern around the true path, especially in the area of the 42 measurements, is evident.

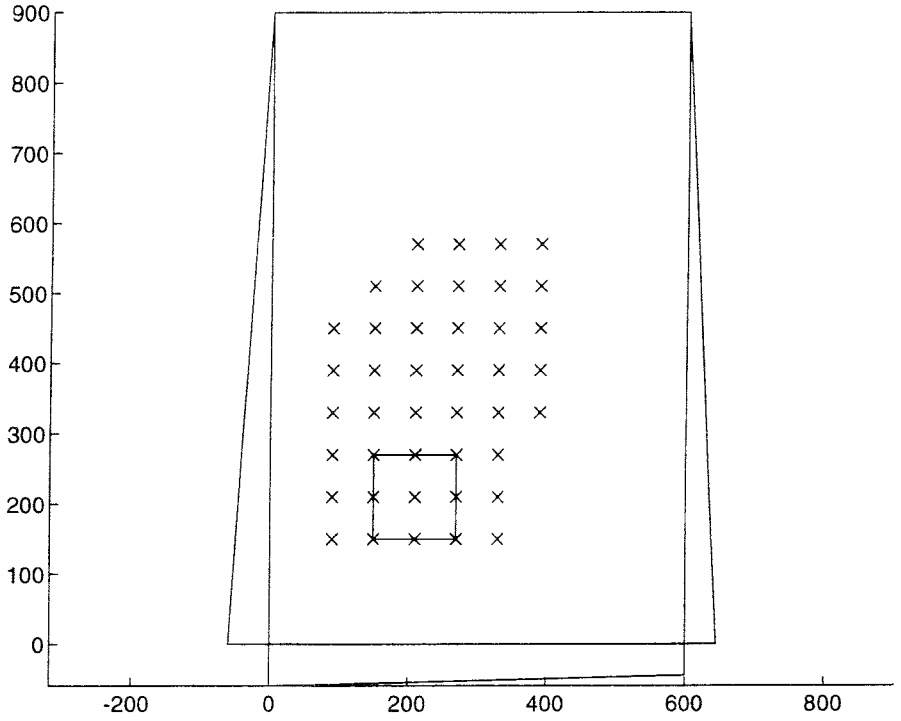

Figure B.1: Computational model with conductivity measurements (x). The external head varies linearly along the boundaries as indicated and is 2 at (0,0), 1.5 at (600,0) and 0 at (0,900) and (600,900). The repository is indicated by the square.

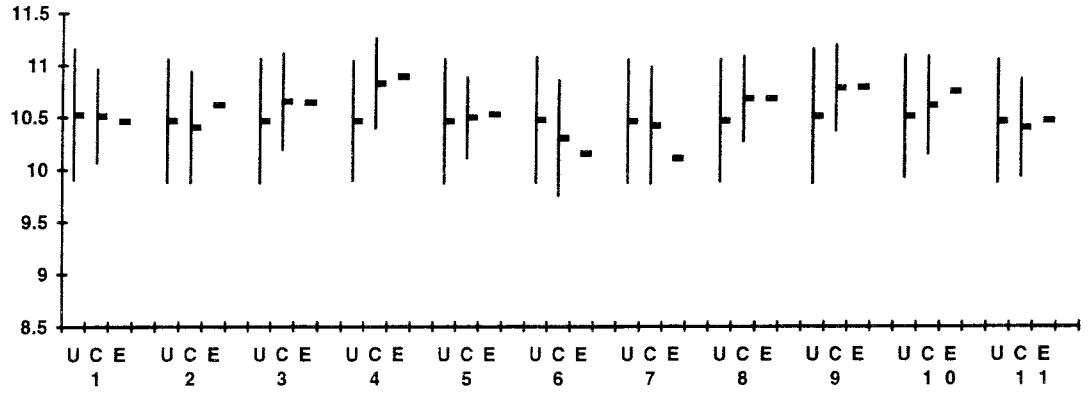

Figure B.2: Computed means and confidence intervals ($\pm 2\sigma$) of the logarithms of particle breakthrough times in the eleven Monte-Carlo simulations. Notation used is : unconditioned fields (U) and fields conditioned on measured conductivities (C). The means for the truth fields are denoted by (E).

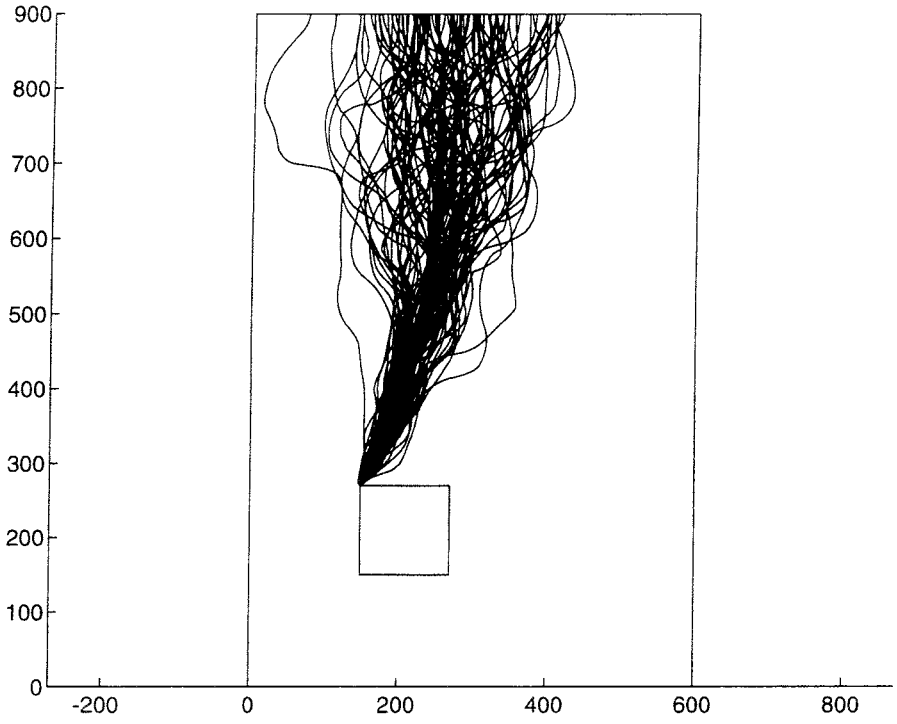

Figure B.3: Traces of particle 5 in the fields conditioned on conductivities, case 4

Appendix C.
Example of problem specification file.

The specification file contains information about geometry, discretization, boundary conditions, variogram, position of measurements etc.. When running the program the name of this file is given interactively.

An example, the input file for the example treated in our previous study (ref[16]), is shown below. It is a MATLAB script file with explanatory comments, which together with some knowledge of MATLAB should make it possible to modify or generate new problem specifications. Note that the percent symbol % denotes a comment.

```
%
%        ----- Computational model ---------
%
%                  ax1, hext(4,:)
%              NY_________________(LX,LY)
%                |                 |
%                |                 |
%                |                 |
%                |                 |
%                |                 |
%          a0y   |     _|__|_      |  a1y
%   hext(1,:)    |      |  |       |  hext(2,:)
%                |  jy _|__|_      |
%                |      |  |       |
%                |     ix          |
%                |_________________|
%           (0,0)  ax0, hext(3,:)
%              1                  NX
%
%      -------------- Input data --------------
%
% # head nodes length
%
  NX = 21;     LX = 600;          dx  = LX/(NX-1);        % x-direction
  NY = 31;     LY = 900;          dy  = LY/(NY-1);        % y-direction
%
% # time steps     time step
%
      nmt = 53;    dt = 181500.0;
%
% Storativity
% -----------
      ss = 1.0e-7;
%
% Conductivity
% ------------
% 10Log-conductivity mean
%
```

```
      ymean = -9;
%
% Fracture zone data
%
% additional log10-conductivity
% log10_conductivity in fracture = ymean + dyfrac
%
      dyfrac = 0;
%
% A fracture zone is specified by two lines. Each line is
% given by a normal (n1 resp. n2) pointing into the fracture
% zone and a point (p1 resp. p2) which it passes through.
% The fracture zone is the intersection of the regions defined
% by the lines.
%
%%    n1 = [ 1 -0.5];   p1 = [0  0];
%%    n2 = [-1 -0.5];   p2 = [300  0];
%
% Semivariogram
% -------------
% model = spheric or exponen

      model = 'spheric';
      semivar(1) = 1;   % variance (sill)
      semivar(2) = 100; % range
      semivar(3) = 100; % in exponential case: distance outside which
%                       the covariance is set zero, default is 3*range
%
%   krnb      = -1 kriging without non-bias condition
%             =  0 kriging in whole domain
%             =  1 kriging in whole ranges
%             =  2 kriging where kriging variance < sill
%
      krnb = 0;
%
% Boundary conditions
% -------------------
% Convection coefficients at the four sides
%
      a0y = 1.0e2;  a1y = 1.0e2;  ax0 = 1.0e2;  ax1 = 1.0e2;
%
% External heads. Linear variation along boundary from val1 to val2
%
%             val1 val2
%
      hext = [   2,   0;            % along line ( 0, 0) to ( 0,LY)
               1.5,   0;            % along line (LX, 0) to (LX,LY)
                 2, 1.5;            % along line ( 0, 0) to (LX, 0)
                 0,   0             % along line ( 0,LY) to (LX,LY)
                        ];
%
% Pumping source
% --------------
% Location in terms of head node indices in matrix
% indq(# sources,2)
%
%             ix   jy;
%
      indq = [11,  16
                       ];    [nsrc,dum] = size(indq);
%
% Time history in matrix q(# sources,# time steps + 1)
% q(:,1) for time 0 and q(:,nmt+1) for time nmt*dt
%
q = 1.0e-6*[ones(nsrc,(nmt-1)*3/4+1) zeros(nsrc,nmt-(nmt-1)*3/4)];
```

```
%
%            q^
%             |
%          -6 |___________
%       10    |           |
%             |           |
%             +-----------|----|->
%             0         3nmt/4  nmt
%
% Initial positions for particles in row vectors x0 and y0
% -------------------------------------------------------
% x-position
      x0=reshape(ones(4,1)*[5*dx,6*dx,7*dx,8*dx],1,16);
% y-position
      y0=reshape([5*dy,6*dy,7*dy,8*dy]'*ones(1,4),1,16);
%
% Stations for head measurements in terms of head node
% indices in matrix indm(# head measurements,2)
% --------------------------------------------
%              ix   jy;
%
      indm = [12   11;
               6   19;
              16   19
                     ];      [nmeas,dum] = size(indm);
%
% Stations for conductivity measurements and pilot points in
% terms of head node indices in matrix
% indpc(# cond.measurements and pilot points,2)
% --------------------------------------------
%              ix jy;
%
      indpc = [10  5;
                4  6;
               12 11;
               11 16;
                6 19;
               16 19;
               17 26
                     ];       [ncmeas,dum] = size(indpc);
%
      indpc=  [indpc;
                8 17;
               14 18;
               11 13
                     ];
      [ncmtot,dum] = size(indpc); npilot = ncmtot-ncmeas;
%
% cstat = 0  no statistics on conductivity fields
%         1  statistics on conductivity fields
%
      cstat = 0;
%
% opt =-2    statistics on conductivity fields only
%      -1    conditioning on conductivities only
%       0    steady state calibration
%       1    steady state + transient calibration
%       2    transient calibration
%
% wss is weight for steady state part of objective function
%
      opt = 2;  wss = 1;
%
% Seed
% ----
```

```
      seed=7;
%
% Method parameters
% -----------------
      itmax = 5;  % Maximum number of CG-iterations
      tol = 0.01; % Tolerance for terminating CG-iterations
%
      ttol=1;     % Tolerance for particle tracing
%
% Save particle traces
% --------------------
%  isave = [1 1 1];
%  tpar  = [2 14];
%
% Truth fields from tru_sta to tru_end are simulated (see below)
% ------------
      tru_sta = 1;  tru_end = 5;
%
% Realizations from real_sta to real_end are simulated
% for truth field tru_sta. Otherwise from 1 to real_end.
%
      real_sta = 1;  real_end = 100;
%
% cont = 1 if continuation of Monte Carlo simulations. Then seeds
%          for truth field tru_sta and realization real_sta are
%          read from file.
%      = 0 otherwise
%
      cont = 0;
%
% The program works as follows:
% -----------------------------
%
% Do i = tru_sta : tru_end
%
%   Save random number.
%   Choose as the truth a realization respecting the variogram.
%   Generate simulated measurements from truth field for the
%   conditioning.
%   If isave exists then
%     particle traces for particles tpar are saved
%     on file 'pm mod_nam(i).mat'
%   else
%     save particle breakthrough times (tfinm), x- and y-coordinates
%     of exit (xfinm, yfinm), measured heads (Meas),
%     mean log10-cond. in measurement- and pilot-points(cmeanmp)
%     and log10-conductivity relative mean in these points (ctrump).
%     on file 'tm mod_nam(i).mat'
%   end
%
%   Do j = real_sta : real_end
%
%     Save random number.
%     Make a realization Yus respecting the variogram.
%     Record particle breakthrough times (tfinn) and
%     x- and y-coordinates of exit (xfinn, yfinn).
%     If isave(1)=1 then
%       particle traces for particles tpar are saved
%       on file 'pn mod_nam(i) j.mat'
%     end
%
%     Make a realization Ycs, based on Yus and conditioned on
%     the conductivities only.
%     Record particle breakthrough times (tfinc) and
%     x- and y-coordinates of exit (xfinc, yfinc).
```

```
%     If isave(2)=1 then
%       particle traces for particles tpar are saved
%       on file 'pc mod_nam(i) j.mat'
%     end
%
%     Make a realization Ycc, based on Yus and conditioned on
%     the conductivities and head measurements. The conditioning
%     on the heads is either a steady state calibration,
%     a transient calibration or a combination of these.
%     Record particle breakthrough times (tfinh), x- and y-
%     coordinates of exit (xfinh, yfinh) and errors in head (err).
%     Also record value of objective function (jvit) and
%     pilot point values (xpit) relative mean for each Cg-iteration.
%     If isave(3)=1 then
%       particle traces for particles tpar are saved
%       on file 'ph mod_nam(i) j.mat'
%     end
%
%     If isave doesn't exist then
%       save particle breakthrough times, x- and y-coordinates of
%       exit and errors in head on file 'tr mod_nam(i) j.mat'.
%       Save objective function and pilot point values on file
%       'jv mod_nam(i) j.mat'.
%     end
%
%   end
%
% end
%
% mod_nam = ['a' 'b' 'c' 'd' 'e' 'f' 'g' 'h' 'i' 'j' 'k' 'l' 'm' ...
%            'n' 'o' 'p' 'q' 'r' 's' 't' 'u' 'v' 'w' 'x' 'y' 'z'];
%
```

List of SKB reports

Annual Reports

1977-78
TR 121
KBS Technical Reports 1 – 120
Summaries
Stockholm, May 1979

1979
TR 79-28
The KBS Annual Report 1979
KBS Technical Reports 79-01 – 79-27
Summaries
Stockholm, March 1980

1980
TR 80-26
The KBS Annual Report 1980
KBS Technical Reports 80-01 – 80-25
Summaries
Stockholm, March 1981

1981
TR 81-17
The KBS Annual Report 1981
KBS Technical Reports 81-01 – 81-16
Summaries
Stockholm, April 1982

1982
TR 82-28
The KBS Annual Report 1982
KBS Technical Reports 82-01 – 82-27
Summaries
Stockholm, July 1983

1983
TR 83-77
The KBS Annual Report 1983
KBS Technical Reports 83-01 – 83-76
Summaries
Stockholm, June 1984

1984
TR 85-01
Annual Research and Development Report 1984
Including Summaries of Technical Reports Issued during 1984. (Technical Reports 84-01 – 84-19)
Stockholm, June 1985

1985
TR 85-20
Annual Research and Development Report 1985
Including Summaries of Technical Reports Issued during 1985. (Technical Reports 85-01 – 85-19)
Stockholm, May 1986

1986
TR 86-31
SKB Annual Report 1986
Including Summaries of Technical Reports Issued during 1986
Stockholm, May 1987

1987
TR 87-33
SKB Annual Report 1987
Including Summaries of Technical Reports Issued during 1987
Stockholm, May 1988

1988
TR 88-32
SKB Annual Report 1988
Including Summaries of Technical Reports Issued during 1988
Stockholm, May 1989

1989
TR 89-40
SKB Annual Report 1989
Including Summaries of Technical Reports Issued during 1989
Stockholm, May 1990

1990
TR 90-46
SKB Annual Report 1990
Including Summaries of Technical Reports Issued during 1990
Stockholm, May 1991

1991
TR 91-64
SKB Annual Report 1991
Including Summaries of Technical Reports Issued during 1991
Stockholm, April 1992

1992
TR 92-46
SKB Annual Report 1992
Including Summaries of Technical Reports Issued during 1992
Stockholm, May 1993

1993
TR 93-34
SKB Annual Report 1993
Including Summaries of Technical Reports Issued during 1993
Stockholm, May 1994

Technical Reports
List of SKB Technical Reports 1994

TR 94-01
Anaerobic oxidation of carbon steel in granitic groundwaters: A review of the relevant literature
N Platts, D J Blackwood, C C Naish
AEA Technology, UK
February 1994

TR 94-02
Time evolution of dissolved oxygen and redox conditions in a HLW repository
Paul Wersin, Kastriot Spahiu, Jordi Bruno
MBT Technología Ambiental, Cerdanyola, Spain
February 1994

TR 94-03
Reassessment of seismic reflection data from the Finnsjön study site and prospectives for future surveys
Calin Cosma[1], Christopher Juhlin[2], Olle Olsson[3]
[1] Vibrometric Oy, Helsinki, Finland
[2] Section for Solid Earth Physics, Department of Geophysics, Uppsala University, Sweden
[3] Conterra AB, Uppsala, Sweden
February 1994

TR 94-04
Final report of the AECL/SKB Cigar Lake Analog Study
Jan Cramer (ed.)[1], John Smellie (ed.)[2]
[1] AECL, Canada
[2] Conterra AB, Uppsala, Sweden
May 1994

TR 94-05
Tectonic regimes in the Baltic Shield during the last 1200 Ma - A review
Sven Åke Larsson[1,2], Eva-Lena Tullborg[2]
[1] Department of Geology, Chalmers University of Technology/Göteborg University
[2] Terralogica AB
November 1993

TR 94-06
First workshop on design and construction of deep repositories - Theme: Excavation through water-conducting major fracture zones Såstaholm Sweden, March 30-31 1993
Göran Bäckblom (ed.), Christer Svemar (ed.)
Swedish Nuclear Fuel & Waste Management Co, SKB
January 1994

TR 94-07
INTRAVAL Working Group 2 summary report on Phase 2 analysis of the Finnsjön test case
Peter Andersson (ed.)[1], Anders Winberg (ed.)[2]
[1] GEOSIGMA, Uppsala, Sweden
[2] Conterra, Göteborg, Sweden
January 1994

TR 94-08
The structure of conceptual models with application to the Äspö HRL Project
Olle Olsson[1], Göran Bäckblom[2], Gunnar Gustafson[3], Ingvar Rhén[4], Roy Stanfors[5], Peter Wikberg[2]
1 Conterra AB
2 SKB
3 CTH
4 VBB/VIAK
5 RS Consulting
May 1994

TR 94-09
Tectonic framework of the Hanö Bay area, southern Baltic Sea
Kjell O Wannäs, Tom Flodén
Institutionen för geologi och geokemi, Stockholms universitet
June 1994

TR 94-10
Project Caesium–An ion exchange model for the prediction of distribution coefficients of caesium in bentonite
Hans Wanner[1], Yngve Albinsson[2], Erich Wieland[1]
[1] MBT Umwelttechnik AG, Zürich, Switzerland
[2] Chalmers University of Technology, Gothenburg, Sweden
June 1994

TR 94-11
Äspö Hard Rock Laboratory Annual Report 1993
SKB
June 1994

TR 94-12
Research on corrosion aspects of the Advanced Cold Process Canister
D J Blackwood, A R Hoch, C C Naish, A Rance, S M Sharland
AEA Technology, Harwell Laboratory, UK
January 1994

TR 94-13
Assessment study of the stresses induced by corrosion in the Advanced Cold Process Canister
A R Hoch, S M Sharland
Chemical Studies Department, Radwaste Disposal Division, AEA Decommissioning and Radwaste, Harwell Laboratory, UK
October 1993

TR 94-14
Performance of the SKB Copper/Steel Canister
Hans Widén[1], Patrik Sellin[2]
[1] Kemakta Konsult AB, Stockholm, Sweden
[2] Svensk Kärnbränslehantering AB, Stockholm, Sweden
September 1994

TR 94-15
Modelling of nitric acid production in the Advanced Cold Process Canister due to irradiation of moist air
J Henshaw
AEA Technology, Decommissioning & Waste Management/Reactor Services, Harwell, UK
January 1994

TR 94-16
Kinetic and thermodynamic studies of uranium minerals. Assessment of the long-term evolution of spent nuclear fuel
Ignasi Casas[1], Jordi Bruno[1], Esther Cera[1], Robert J Finch[2], Rodney C Ewing[2]
[1] MBT Tecnología Ambiental, Cerdanyola, Spain
[2] Department of Earth and Planetary Sciences, University of New Mexico, Albuquerque, NM, USA
October 1994

TR 94-17
Summary report of the experiences from TVO's site investigations
Antti Öhberg[1], Pauli Saksa[2], Henry Ahokas[2], Paula Ruotsalainen[2], Margit Snellman[3]
[1] Saanio & Riekkola Consulting Engineers, Helsinki, Finland
[2] Fintact Ky, Helsinki, Finland
[3] Imatran Voima Oy, Helsinki, Finland
May 1994

TR 94-18
AECL strategy for surface-based investigations of potential disposal sites and the development of a geosphere model for a site
S H Whitaker, A Brown, C C Davison, M Gascoyne, G S Lodha, D R Stevenson, G A Thorne, D Tomsons
AECL Research, Whiteshell Laboratories, Pinawa, Manitoba, Canada
May 1994

TR 94-19
Deep drilling KLX 02. Drilling and documentation of a 1700 m deep borehole at Laxemar, Sweden
O Andersson
VBB VIAK AB, Malmö
August 1994

TR 94-20
Technology and costs for decommissioning the Swedish nuclear power plants
Swedish Nuclear Fuel and Waste Management Co, Stockholm, Sweden
June 1994

TR 94-21
Verification of HYDRASTAR: Analysis of hydraulic conductivity fields and dispersion
S T Morris, K A Cliffe
AEA Technology, Harwell, UK
October 1994

TR 94-22
Evaluation of stationary and non-stationary geostatistical models for inferring hydraulic conductivity values at Äspö
Paul R La Pointe
Golder Associates Inc., Seattle, WA, USA
November 1994

TR 94-23
PLAN 94
Costs for management of the radioactive waste from nuclear power production
Swedish Nuclear Fuel and Waste Management Co
June 1994

TR 94-24
Äspö Hard Rock Laboratory
Feasibility and usefulness of site investigation methods. Experiences from the pre-investigation phase
Karl-Erik Almén (ed.)[1], Pär Olsson[2], Ingvar Rhén[3], Roy Stanfors[4], Peter Wikberg[5]
[1] KEA GEO-Konsult
[2] SKANSKA
[3] VBB/VIAK
[4] RS Consulting
[5] SKB
August 1994

TR 94-25

Kinetic modelling of bentonite-canister interaction. Long-term predictions of copper canister corrosion under oxic and anoxic conditions

Paul Wersin, Kastriot Spahiu, Jordi Bruno
MBT Tecnología Ambiental, Cerdanyola, Spain
September 1994

TR 94-26

A surface chemical model of the bentonite-water interface and its implications for modelling the near field chemistry in a repository for spent fuel

Erich Wieland[1], Hans Wanner[1], Yngve Albinsson[2], Paul Wersin[3], Ola Karnland[4]
[1] MBT Umwelttechnik AG, Zürich, Switzerland
[2] Chalmers University of Technology, Gothenburg, Sweden
[3] MBT Tecnología Ambiental, Cerdanyola, Spain
[4] Clay Technology AB, Lund, Sweden
July 1994

TR 94-27

Experimental study of strontium sorption on fissure filling material

Trygve E Eriksen, Daqing Cui
Department of Chemistry, Nuclear Chemistry, Royal Institute of Technology, Stockholm, Sweden
December 1994

TR 94-28

Scenario development methodologies

Torsten Eng[1], John Hudson[2], Ove Stephansson[3], Kristina Skagius[4], Marie Winborgh[4]
[1] Swedish Nuclear Fuel & Waste Management Co, Stockholm, Sweden
[2] Rock Engineering Consultants, Welwyn Garden City, Herts, UK
[3] Div. of Engineering Geology, Royal Institute of Technology, Stockholm, Sweden
[4] Kemakta, Stockholm, Sweden
November 1994

TR 94-29

Heat conductivity of buffer materials

Lennart Börgesson, Anders Fredrikson, Lars-Erik Johannesson
Clay Technology AB, Lund, Sweden
November 1994